

REGULARIZATION METHODS FOR THE NUMERICAL SOLUTION OF THE DIVERGENCE EQUATION $\nabla \cdot \mathbf{u} = f^*$

Alexandre Caboussat

University of Houston, Department of Mathematics, Houston, Texas, USA

Email: caboussat@math.uh.edu

Haute Ecole de Gestion, Genève, Switzerland

Email: alexandre.caboussat@hesge.ch

Roland Glowinski

University of Houston, Department of Mathematics, Houston, Texas, USA

Email: roland@math.uh.edu

Abstract

The problem of finding a L^∞ -bounded two-dimensional vector field whose divergence is given in L^2 is discussed from the numerical viewpoint. A systematic way to find such a vector field is to introduce a non-smooth variational problem involving a L^∞ -norm. To solve this problem from calculus of variations, we use a method relying on a well-chosen augmented Lagrangian functional and on a mixed finite element approximation. An Uzawa algorithm allows to decouple the differential operators from the nonlinearities introduced by the L^∞ -norm, and leads to the solution of a sequence of Stokes-like systems and of an infinite family of local nonlinear problems. A simpler method, based on a L^2 -regularization is also considered. Numerical experiments are performed, making use of appropriate numerical integration techniques when non-smooth data are considered; they allow to compare the merits of the two approaches discussed in this article and to show the ability of the related methods at capturing L^∞ -bounded solutions.

Mathematics subject classification: 65N30, 65K10, 65J20, 49K20, 90C47.

Key words: Divergence equation, Bounded solutions, Regularization methods, Augmented Lagrangian, Uzawa algorithm, Nonlinear variational problems.

1. Introduction and Motivations

The purpose of this article is to investigate the numerical solution of the following problem

$$\text{Find } \mathbf{u} \in (L^\infty(\Omega) \cap W^{1,p}(\Omega))^2 \text{ such that } \nabla \cdot \mathbf{u} = f \quad \text{in } \Omega \subset \mathbb{R}^2, \quad (1.1)$$

where $f \in L^p(\Omega)$ is given. This problem is under-determined in the sense that the solution is defined up to the addition of an arbitrary function with zero curl. It is common to look for a solution that is the *gradient of a potential function* (as in electromagnetism for example). The resulting potential function is therefore the solution of a Poisson equation.

However, when $p = 1$ or $p = +\infty$, obtaining a solution which is the gradient of a potential function is not necessarily possible, see, e.g., [1, 2]. Moreover, when considering $p = 2$, the gradient of such a potential function obtained by solving a Poisson equation is not necessarily bounded [3]. Therefore, we focus hereafter on the so-called *non-smooth case* that consists in enforcing bounded solutions instead of gradients of potential functions.

* Received June 8, 2011 / Revised version received November 15, 2011 / Accepted December 14, 2011 / Published online July 6, 2012 /

This problem has been studied from the theoretical viewpoint in [1, 2, 4], with a particular emphasis on the torus domain, using arguments from [5]. Regularity issues have been discussed in [6, 7]. The case $p = 1$ is partially discussed in [8]. In [1], it is shown that one can actually replace $L^\infty(\Omega)$ by $C^0(\overline{\Omega})$ in (1.1) if $p = 2$.

In order to search for a bounded solution, we introduce an equivalent variational formulation. More precisely, for $g > 0$ a given parameter and $f \in L^p(\Omega)$ given, we look for the solution of

$$\inf_{\mathbf{v} \in \mathbf{E}_f} \left[\frac{1}{p} \int_{\Omega} |\nabla \mathbf{v}|^p \, d\mathbf{x} + g \|\mathbf{v}\|_{\infty} \right], \tag{1.2}$$

where $\|\mathbf{v}\|_{\infty} := \text{ess sup}_{\mathbf{x} \in \Omega} \sqrt{v_1^2 + v_2^2}$, for all $\mathbf{v} = \{v_1, v_2\}$ and

$$\mathbf{E}_f = \{ \mathbf{v} \in (W^{1,p}(\Omega) \cap L^\infty(\Omega))^2, \nabla \cdot \mathbf{v} = f \text{ in } \Omega \}.$$

This choice of the objective function allows to enforce the appropriate regularity of the solution. The minimizer of this constrained variational problem provides a solution to the divergence equation (1.1) with the appropriate regularity, and allows to “fix the constant” in the family of solutions of the divergence equation. From now on, we focus on the case $p = 2$ ($f \in L^2(\Omega)$). Actually for some test problems, we will assume that $f \in L^p(\Omega)$ with $1 \leq p < 2$.

Numerical methods for such non-smooth variational problems require an appropriate treatment of the non-Hilbertian features introduced by the sup-norm. Such numerical algorithms for non-smooth problems have been developed in the framework of fully nonlinear elliptic problems [9, 10], or for generalized eigenvalue problems [11–14].

We advocate an augmented Lagrangian algorithm that allows to decouple the solution of a non-smooth variational problem into the solution of a sequence of Stokes-like systems (solved for instance with stabilized continuous finite elements [15, 16]), and non-smooth problems solved locally (namely at each grid point of a finite element triangulation). The treatment of the sup-norm is achieved with a *duality* approach that has already been successfully applied in [17].

In a second part, we will address a L^2 -regularization of problem (1.1) and compare with the previous approach. Namely, for $\gamma > 0$, we look for a solution of

$$\inf_{\mathbf{v} \in \mathbf{T}_f} \left[\frac{1}{2} \int_{\Omega} |\nabla \mathbf{v}|^2 \, d\mathbf{x} + \frac{\gamma}{2} \int_{\Omega} |\mathbf{v}|^2 \, d\mathbf{x} \right] \tag{1.3}$$

with

$$\mathbf{T}_f = \{ \mathbf{v} \in (H^1(\Omega))^2, \nabla \cdot \mathbf{v} = f \text{ in } \Omega \}.$$

This variational problem leads to the solution of a Stokes system.

Regularization methods are quite common in the literature as basic tools for the solution of ill-posed problems. They are well-known in the framework of inverse problems, starting with [18–21]. In [22, 23], classical questions such as the appropriate choice of parameters and generalizations to family of regularization methods have been addressed. Many advances have been recently made when relying on non-smooth regularization terms using L^1 or L^∞ norms (or their algebraic equivalents), see, e.g., [24, 25]. This approach has already been used by the authors in the framework of *non-smooth* problems, see, e.g., [17, 26].

This article is organized as follows: Section 2 details the generic model problem and provides some existence results as well as the description of some properties of the solution of (1.2). In Section 3, an augmented Lagrangian algorithm *à la Uzawa* is described. The discrete equivalent of this algorithm, obtained after discretization with continuous mixed piecewise linear finite elements, is detailed in Section 4. Numerical experiments with the L^∞ -regularization are performed in Section 5, for smooth and non-smooth data, and a computational investigation of the convergence of the approximations (with respect to the mesh size) is achieved. Section 6 details the L^2 -regularization method, and presents numerical results to compare both approaches.

2. A Non-Smooth Variational Problem

2.1. Model problem and generalities

Let $\Omega \subset \mathbb{R}^2$ be a bounded domain, with a smooth boundary $\Gamma = \partial\Omega$, and $f \in L^2(\Omega)$. The problem of interest is to find a function $\mathbf{u} : \Omega \rightarrow \mathbb{R}^2$ such that

$$\mathbf{u} \in (H^1(\Omega) \cap C^0(\overline{\Omega}))^2, \quad \nabla \cdot \mathbf{u} = f. \tag{2.1}$$

The following existence result for a solution to (2.1) is extracted from [1, 2]:

Theorem 2.1 (Existence) *Problem (2.1) has a solution, not necessarily unique. Moreover, if Ω is convex and Γ is smooth enough, there exists a constant C such that:*

$$\|\mathbf{u}\|_\infty + \|\mathbf{u}\|_{(H^1(\Omega))^2} \leq C \|f\|_{L^2(\Omega)}.$$

Let us denote $\|\cdot\|_\infty := \|\cdot\|_{(L^\infty(\Omega))^2}$, and let $g > 0$ be a given positive number. First we define the set:

$$\mathbf{S}_f = \left\{ \mathbf{v} \in (H^1(\Omega) \cap C^0(\overline{\Omega}))^2 : \nabla \cdot \mathbf{v} = f \text{ in } \Omega \right\}; \tag{2.2}$$

next, g being a given positive number, we define the functional

$$J(\mathbf{v}) = \frac{1}{2} \int_{\Omega} |\nabla \mathbf{v}|^2 \, d\mathbf{x} + g \|\mathbf{v}\|_\infty.$$

It follows from Theorem 2.1 that the *non-smooth variational problem*:

$$\text{Find } \mathbf{u} \in \mathbf{S}_f \text{ such that } J(\mathbf{u}) \leq J(\mathbf{v}), \quad \forall \mathbf{v} \in \mathbf{S}_f, \tag{2.3}$$

has a solution. The formulation (2.3) enforces the admissible solution to be L^∞ -bounded. The positive coefficient g allows to enforce the L^∞ -boundedness requirement. The uniqueness of the solution is enforced in some case, as shown by the following

Theorem 2.2 (Uniqueness) *For $g > 0$ a given parameter, the solution of (2.3) is unique. Moreover, if g_1 and g_2 are two given parameters, and \mathbf{u}_1 and \mathbf{u}_2 are the corresponding (unique) solutions of (2.3) where the objective functionals are associated with g_1 and g_2 respectively, then:*

$$(g_1 - g_2) (\|\mathbf{u}_2\|_\infty - \|\mathbf{u}_1\|_\infty) \geq 0;$$

i.e. *the sup-norm of the solution is a decreasing function of the parameter g .*

Proof. For $g > 0$ given, let us assume that (2.3) admits two solutions \mathbf{u}_1 and \mathbf{u}_2 . It follows from, e.g., [27, 28] that \mathbf{u}_1 and \mathbf{u}_2 satisfy the following *variational inequalities*

$$\int_{\Omega} \nabla \mathbf{u}_1 : \nabla(\mathbf{v} - \mathbf{u}_1) \, d\mathbf{x} + g (\|\mathbf{v}\|_\infty - \|\mathbf{u}_1\|_\infty) \geq 0, \quad \forall \mathbf{v} \in \mathbf{S}_f \tag{2.4}$$

and

$$\int_{\Omega} \nabla \mathbf{u}_2 : \nabla(\mathbf{v} - \mathbf{u}_2) \, d\mathbf{x} + g (\|\mathbf{v}\|_\infty - \|\mathbf{u}_2\|_\infty) \geq 0, \quad \forall \mathbf{v} \in \mathbf{S}_f, \tag{2.5}$$

respectively. We take $\mathbf{v} = \mathbf{u}_2$ in (2.4), $\mathbf{v} = \mathbf{u}_1$ in (2.5), and add both relations to obtain

$$- \int_{\Omega} |\nabla(\mathbf{u}_2 - \mathbf{u}_1)|^2 \, d\mathbf{x} \geq 0,$$

which implies in turn that $\nabla(\mathbf{u}_2 - \mathbf{u}_1) = \mathbf{0}$, that is $\mathbf{u}_2 - \mathbf{u}_1 = \mathbf{C}$, where \mathbf{C} is a constant two-dimensional vector, and (since $\nabla \mathbf{u}_1 = \nabla \mathbf{u}_2$) that

$$\|\mathbf{u}_1\|_\infty = \|\mathbf{u}_2\|_\infty. \tag{2.6}$$

Suppose that $\mathbf{C} \neq \mathbf{0}$, we have then

$$\mathbf{u}_1(\mathbf{x}) \neq \mathbf{u}_2(\mathbf{x}), \quad \forall \mathbf{x} \in \Omega. \tag{2.7}$$

Denote by $\mathbf{w}(= \{w_1, w_2\})$ the vector-valued function $\frac{1}{2}(\mathbf{u}_1 + \mathbf{u}_2)$; we clearly have

$$\nabla \mathbf{w} = \nabla \mathbf{u}_1 = \nabla \mathbf{u}_2. \tag{2.8}$$

Suppose now that the (continuous) function $\mathbf{x} \rightarrow |w_1(\mathbf{x})|^2 + |w_2(\mathbf{x})|^2$ reaches its maximum value over Ω at $\hat{\mathbf{x}}$; we have then

$$\|\mathbf{w}\|_\infty^2 = |\mathbf{w}(\hat{\mathbf{x}})|^2. \tag{2.9}$$

where $|\boldsymbol{\xi}| = \sqrt{\xi_1^2 + \xi_2^2}$, for all $\boldsymbol{\xi} = \{\xi_1, \xi_2\} \in \mathbb{R}^2$. It follows from (2.6), (2.7), (2.9), and from the *strict convexity* of the function $\boldsymbol{\xi} \rightarrow |\boldsymbol{\xi}|^2$, that

$$\begin{aligned} \|\mathbf{w}\|_\infty^2 &= |\mathbf{w}(\hat{\mathbf{x}})|^2 < \frac{1}{2} \left(|\mathbf{u}_1(\hat{\mathbf{x}})|^2 + |\mathbf{u}_2(\hat{\mathbf{x}})|^2 \right) \\ &\leq \frac{1}{2} \left(\|\mathbf{u}_1\|_\infty^2 + \|\mathbf{u}_2\|_\infty^2 \right) = \|\mathbf{u}_1\|_\infty^2 = \|\mathbf{u}_2\|_\infty^2. \end{aligned}$$

We have thus shown that

$$\|\mathbf{w}\|_\infty^2 < \|\mathbf{u}_1\|_\infty^2 = \|\mathbf{u}_2\|_\infty^2. \tag{2.10}$$

Combining (2.10) with (2.6) and (2.8), we obtain that $J(\mathbf{w}) < J(\mathbf{u}_1) = J(\mathbf{u}_2)$, which contradicts the fact that \mathbf{u}_1 and \mathbf{u}_2 are solutions of problem (2.3). We have thus $\mathbf{C} = \mathbf{0}$, which implies uniqueness.

Let us now consider g_1 and g_2 two positive parameters. The relations corresponding to (2.4) (with $g = g_1$) and (2.5) (with $g = g_2$) lead to

$$-\int_{\Omega} |\nabla(\mathbf{u}_2 - \mathbf{u}_1)|^2 d\mathbf{x} + (g_1 - g_2) (\|\mathbf{u}_2\|_\infty - \|\mathbf{u}_1\|_\infty) \geq 0,$$

and conclusion follows, namely $\|\mathbf{u}_2\|_\infty \geq \|\mathbf{u}_1\|_\infty$ if $g_2 \leq g_1$. □

Actually, numerical results suggest that the solution \mathbf{u} is independent of the choice of the parameter g .

2.2. On the well-posedness of the problem and the singular cases

For a given $f \in L^2(\Omega)$, a well-posed problem (arising, e.g., in electromagnetism) consists in finding a function $\mathbf{u} \in (H^1(\Omega))^2$ that satisfies

$$\nabla \cdot \mathbf{u} = f \text{ in } \Omega, \quad \nabla \times \mathbf{u} = 0 \text{ in } \Omega,$$

together with appropriate boundary conditions. According to the *Helmholtz-Hodge decomposition*, every function $\mathbf{u} \in (L^2(\Omega))^2$ has an orthogonal decomposition into the gradient of a potential function and the curl of a vector-valued function (see, e.g., [29, Chapter I]); this result implies that the solution of this problem satisfies $\mathbf{u} = \nabla \Phi$ in Ω , where $\Phi \in H^2(\Omega)$ is a *potential function*. Another consequence of this decomposition is that, if \mathbf{u} satisfies (2.1), then the potential function Φ satisfies the Poisson equation $\Delta \Phi = f$ in Ω . However, when $f \in L^2(\Omega) \setminus L^\infty(\Omega)$, the function $\mathbf{u} = \nabla \Phi$ is not necessarily bounded, since the solution Φ of this Poisson equation is in $H^2(\Omega)$ but has no more regularity in general. Hence $\mathbf{u} \in (H^1(\Omega))^2$, but it may happen that $\mathbf{u} \notin (L^\infty(\Omega))^2$ (for $\Omega \subset \mathbb{R}^2$). Therefore the additional condition $\nabla \times \mathbf{u} = 0$ does not guarantee the required regularity on the solution of our problem of interest.

In the variational framework in which we investigate the solution of (2.1), the condition $\nabla \times \mathbf{u} = 0$ is disregarded and, instead, we look for the function that minimizes the 'energy'

$J(\cdot)$. Numerical experiments in Section 5 actually suggest that this solution may still be the gradient of a potential function.

The most interesting case therefore occurs when $f \in L^2(\Omega) \setminus L^\infty(\Omega)$. In particular, we are going to investigate the following case of a radial function with a point singularity:

$$f(\mathbf{x}) = f(x_1, x_2) = \frac{1}{((x_1 - x_1^0)^2 + (x_2 - x_2^0)^2)^{s/2}}, \quad s > 0, \tag{2.11}$$

where $(x_1^0, x_2^0) \in \Omega$ and $s > 0$ arbitrary.

Lemma 2.1. *When $\Omega = \mathcal{D}_1$ is the unit disk $\{(x_1, x_2) \in \mathbb{R}^2 : x_1^2 + x_2^2 < 1\}$ and $(x_1^0, x_2^0) = (0, 0)$, the function f defined as in (2.11) satisfies the property: $f \in L^q(\mathcal{D}_1)$ if $s < \frac{2}{q}$, for $q > 0$. In particular, $f \in L^2(\mathcal{D}_1)$ if $s < 1$.*

Proof. By definition, $f \in L^q(\mathcal{D}_1)$ if $\int_{\mathcal{D}_1} |f(x_1, x_2)|^q dx_1 dx_2 < +\infty$. This implies

$$\begin{aligned} \infty &> \int_{\mathcal{D}_1} |f(x_1, x_2)|^q dx_1 dx_2 = \int_0^{2\pi} \int_0^1 |f(r, \theta)|^q r dr d\theta = \int_0^{2\pi} \int_0^1 \frac{1}{r^{sq}} r dr d\theta \\ &> 2\pi \int_0^1 \frac{1}{r^{sq}} r dr = 2\pi \int_0^1 r^{1-sq} dr. \end{aligned}$$

The function r^{1-sq} is integrable over $(0, 1)$ if $1 - sq > -1$ and conclusion follows. □

2.3. Theoretical results

In this Section, we present some results about the solution of (2.3) in various, smooth and non-smooth, cases. These results will be confirmed by the numerical experiments reported in Section 5, and help to understand the nature of the solution. When the data f is smooth (for instance, we will consider $f = 2$), partial information about the solution is the topic of the following result.

Proposition 2.1 (Case of data f with radial invariance) *For any $\Omega \subset \mathbb{R}^2$ with a smooth boundary, let us consider $f \in L^2(\Omega)$ that is radially symmetric with respect to $(x_1^0, x_2^0) \in \Omega$. Assume that the solution $\mathbf{u} \in (H^1(\Omega) \cap C^0(\overline{\Omega}))^2$ of (2.3) has the form*

$$\mathbf{u}(x_1, x_2) = \varphi \left(\sqrt{(x_1 - x_1^0)^2 + (x_2 - x_2^0)^2} \right) \begin{pmatrix} x_1 - x_1^0 \\ x_2 - x_2^0 \end{pmatrix},$$

where $\varphi(\cdot)$ is a smooth function. Then it should read as

$$\varphi(r) = \frac{1}{r^2} \int_0^r f(t)t dt. \tag{2.12}$$

Proof. For \mathbf{u} given by the assumptions of the Theorem, we have

$$\nabla \cdot \mathbf{u} = 2\varphi(r) + \varphi'(r)r, \quad \text{with } r = \sqrt{(x_1 - x_1^0)^2 + (x_2 - x_2^0)^2}.$$

If f is radially symmetric, $f = f(r)$, and the relation $\nabla \cdot \mathbf{u} = f$ implies the ordinary differential equation $2\varphi(r) + \varphi'(r)r = f(r)$, for $0 < r < 1$. Solving this equation, with, e.g., the boundary condition $\varphi(0) = 0$, gives (2.12). □

In particular, for the case $f = 2$, we obtain $\varphi(r) = 1$ and $\mathbf{u}(x_1, x_2) = (x_1 - x_1^0, x_2 - x_2^0)^T$, implying (by symmetry) that $\mathbf{u}(x_1, x_2) = (x_1, x_2)^T$ when Ω is the unit disk

$$\mathcal{D}_1 = \left\{ \mathbf{x} = (x_1, x_2) \in \mathbb{R}^2 : x_1^2 + x_2^2 < 1 \right\},$$

and $\mathbf{u}(x_1, x_2) = (x_1 - \frac{1}{2}, x_2 - \frac{1}{2})^T$ when Ω is the unit square $\Omega_s = (0, 1)^2$. When $f(r) = r^{-s}$, which corresponds to (2.11), one obtains

$$\varphi(r) = \frac{r^{-s}}{2-s}, \quad \text{and} \quad \mathbf{u}(x_1, x_2) = \frac{1}{r^s} \frac{1}{2-s} \begin{pmatrix} x_1 - x_1^0 \\ x_2 - x_2^0 \end{pmatrix}. \quad (2.13)$$

A consequence of (2.13) is the following result.

Proposition 2.2. *The solution \mathbf{u} of (2.3) with f given by (2.11) is continuous when $s < 1$, but discontinuous when $s = 1$.*

Proof. Starting from (2.13) it is easy to see that, when $s < 1$,

$$\lim_{(x_1, x_2) \rightarrow (x_1^0, x_2^0)} \mathbf{u}(x_1, x_2) = \mathbf{0}.$$

The limit is not defined when $s = 1$ (actually, when $s = 1$, the limit depends on the slope $(x_2 - x_2^0)/(x_1 - x_1^0)$ with which (x_1, x_2) tends to (x_1^0, x_2^0)). \square

We have just shown that, if $f(r) = r^{-1}$ (i.e. $f(\mathbf{x}) = 1/|\mathbf{x}|$), then $f \notin L^2(\Omega)$ if $(x_1^0, x_2^0) \in \Omega \subset \mathbb{R}^2$. However, $f \in L^p(\Omega)$ for $1 \leq p < 2$. Although the results of [1] do not apply to the associated problem (1.1), this particular case has been investigated numerically in Section 5.

In the sequel, we address the numerical solution of the variational problem (2.3) by an *augmented Lagrangian algorithm*.

3. An Augmented Lagrangian Approach

3.1. Augmented lagrangian and saddle-point problem

Let us focus first on the L^∞ -regularization given by (2.3). An alternative approach, based on the L^2 -regularization (see (1.3)) is discussed in Section 6. Problem (2.3) is equivalent to:

$$\text{Find } \{\mathbf{u}, \mathbf{p}\} \in \mathbf{W}_f \text{ such that } j(\mathbf{u}, \mathbf{p}) \leq j(\mathbf{v}, \mathbf{q}), \quad \forall \{\mathbf{v}, \mathbf{q}\} \in \mathbf{W}_f, \quad (3.1)$$

where

$$\mathbf{W}_f = \left\{ \{\mathbf{v}, \mathbf{q}\} \in (H^1(\Omega))^2 \times (L^\infty(\Omega))^2 : \nabla \cdot \mathbf{v} = f \text{ in } \Omega, \mathbf{v} - \mathbf{q} = \mathbf{0} \text{ in } \Omega \right\}, \quad (3.2)$$

and

$$j(\mathbf{v}, \mathbf{q}) = \frac{1}{2} \int_{\Omega} |\nabla \mathbf{v}|^2 \, d\mathbf{x} + g \|\mathbf{q}\|_{\infty}.$$

The introduction of the vector-valued function \mathbf{q} allows to decouple the boundedness constraint from the divergence equation. The augmented Lagrangian method discussed here is inspired from [27, 30]; it consists in searching for a *saddle point* of the following augmented Lagrangian functional:

$$\mathcal{L}_r(\mathbf{v}, \mathbf{q}; \boldsymbol{\mu}) = j(\mathbf{v}, \mathbf{q}) + \frac{r}{2} \int_{\Omega} |\mathbf{v} - \mathbf{q}|^2 \, d\mathbf{x} + \int_{\Omega} \boldsymbol{\mu} \cdot (\mathbf{v} - \mathbf{q}) \, d\mathbf{x}, \quad (3.3)$$

where $\boldsymbol{\mu}$ is a Lagrange multiplier. Namely, we are looking for $\{\mathbf{u}, \mathbf{p}, \boldsymbol{\lambda}\} \in \mathbf{V}_f \times (L^\infty(\Omega))^2 \times (L^2(\Omega))^2$ such that

$$\mathcal{L}_r(\mathbf{u}, \mathbf{p}; \boldsymbol{\mu}) \leq \mathcal{L}_r(\mathbf{u}, \mathbf{p}; \boldsymbol{\lambda}) \leq \mathcal{L}_r(\mathbf{v}, \mathbf{q}; \boldsymbol{\lambda}), \quad (3.4)$$

for all $\{\mathbf{v}, \mathbf{q}; \boldsymbol{\mu}\} \in \mathbf{V}_f \times (L^\infty(\Omega))^2 \times (L^2(\Omega))^2$, where $\mathbf{V}_f = \{\mathbf{v} \in (H^1(\Omega))^2 : \nabla \cdot \mathbf{v} = f \text{ in } \Omega\}$.

Theorem 3.1. *Any solution $\{\mathbf{u}, \mathbf{p}, \boldsymbol{\lambda}\}$ of the saddle-point problem (3.4) is such that \mathbf{u} solves (2.3) and $\mathbf{p} = \mathbf{u}$.*

Proof. The first (left) inequality in (3.4) implies that

$$\int_{\Omega} (\boldsymbol{\lambda} - \boldsymbol{\mu}) \cdot (\mathbf{u} - \mathbf{p}) d\mathbf{x} \geq 0,$$

for all $\boldsymbol{\mu} \in (L^2(\Omega))^2$, which implies $\mathbf{u} = \mathbf{p}$, a.e. in Ω . Starting from this property, the second (right) inequality in (3.4) reads

$$j(\mathbf{u}, \mathbf{p}) \leq j(\mathbf{v}, \mathbf{q}) + \frac{r}{2} \int_{\Omega} |\mathbf{v} - \mathbf{q}|^2 d\mathbf{x} + \int_{\Omega} \boldsymbol{\lambda} \cdot (\mathbf{v} - \mathbf{q}) d\mathbf{x},$$

for all $\{\mathbf{v}, \mathbf{q}\} \in \mathbf{V}_f \times (L^\infty(\Omega))^2$; in particular, by taking $\mathbf{q} = \mathbf{v}$, one obtains

$$J(\mathbf{u}) = j(\mathbf{u}, \mathbf{u}) \leq j(\mathbf{v}, \mathbf{v}) = J(\mathbf{v}), \quad \forall \mathbf{v} \in \mathbf{S}_f,$$

and conclusion follows. \square

The following *Uzawa algorithm* is advocated to solve (3.4). It is inspired from the so-called *ALG2* algorithm presented in [30].

3.2. Uzawa algorithm

An Uzawa-Douglas-Rachford type algorithm reads as follows: let $\mathbf{u}^{-1} \in \mathbf{V}_f$ and $\boldsymbol{\lambda}^0 \in (L^2(\Omega))^2$ be arbitrary given functions. Then, for $n \geq 0$, $\{\mathbf{u}^{n-1}, \boldsymbol{\lambda}^n\}$ being known, the iterates $\mathbf{p}^n, \mathbf{u}^n$ and $\boldsymbol{\lambda}^{n+1}$ are computed as follows:

(a) Solve

$$\mathbf{p}^n = \arg \inf_{\mathbf{q} \in (L^\infty(\Omega))^2} \mathcal{L}_r(\mathbf{u}^{n-1}, \mathbf{q}; \boldsymbol{\lambda}^n). \quad (3.5)$$

(b) Solve

$$\mathbf{u}^n = \arg \inf_{\mathbf{v} \in \mathbf{V}_f} \mathcal{L}_r(\mathbf{v}, \mathbf{p}^n; \boldsymbol{\lambda}^n). \quad (3.6)$$

(c) Update the multipliers $\boldsymbol{\lambda}^n \in (L^2(\Omega))^2$:

$$\boldsymbol{\lambda}^{n+1} = \boldsymbol{\lambda}^n + r(\mathbf{u}^n - \mathbf{p}^n), \quad (3.7)$$

until convergence is reached. Typically the stopping criterion is $\|\mathbf{u}^n - \mathbf{u}^{n-1}\|_{(L^2(\Omega))^2} < \varepsilon$, where ε is a given tolerance. The augmented Lagrangian algorithm produces a sequence of iterates $\{\mathbf{u}^n\}_{n \geq 0}$ that eventually converges to the function realizing the infimum of (2.3). The updating operation described in (3.7) being straightforward, we will detail in the following sections the solution of the sub-problems (3.5) and (3.6).

3.3. On the solution of the sub-problem (3.5)

Problem (3.5) can be written as

$$\mathbf{p}^n = \arg \inf_{\mathbf{q} \in (L^\infty(\Omega))^2} \left[\frac{r}{2} \int_{\Omega} |\mathbf{q}|^2 d\mathbf{x} + g \|\mathbf{q}\|_\infty - \int_{\Omega} \mathbf{X}^n \cdot \mathbf{q} d\mathbf{x} \right], \quad (3.8)$$

where $\mathbf{X}^n := r\mathbf{u}^{n-1} + \boldsymbol{\lambda}^n \in (L^2(\Omega))^2$. We first observe that

$$\|\mathbf{q}\|_\infty = \sup_{\boldsymbol{\mu} \in \boldsymbol{\Lambda}} \int_{\Omega} \boldsymbol{\mu} \cdot \mathbf{q} d\mathbf{x},$$

where

$$\boldsymbol{\Lambda} = \left\{ \boldsymbol{\mu} \in (L^2(\Omega))^2 : \int_{\Omega} |\boldsymbol{\mu}| d\mathbf{x} \leq 1 \right\}$$

(see, e.g., [17]). Problem (3.8) is thus equivalent to

$$\inf_{\mathbf{q} \in (L^\infty(\Omega))^2} \left\{ \sup_{\boldsymbol{\mu} \in \Lambda} \left[\frac{r}{2} \int_{\Omega} |\mathbf{q}|^2 dx + g \int_{\Omega} \boldsymbol{\mu} \cdot \mathbf{q} dx - \int_{\Omega} \mathbf{X}^n \cdot \mathbf{q} dx \right] \right\}. \quad (3.9)$$

which is equivalent to

$$\sup_{\boldsymbol{\mu} \in \Lambda} \left\{ \inf_{\mathbf{q} \in (L^\infty(\Omega))^2} \left[\frac{r}{2} \int_{\Omega} |\mathbf{q}|^2 dx + g \int_{\Omega} \boldsymbol{\mu} \cdot \mathbf{q} dx - \int_{\Omega} \mathbf{X}^n \cdot \mathbf{q} dx \right] \right\}. \quad (3.10)$$

For a given $\boldsymbol{\mu}$, the minimization problem is a quadratic problem for the variable $\mathbf{q} \in (L^\infty(\Omega))^2$, whose explicit solution is given by

$$\mathbf{p}^n(\boldsymbol{\mu}) = \frac{1}{r} (\mathbf{X}^n - g\boldsymbol{\mu}). \quad (3.11)$$

It remains to compute the supremum of (3.10) in terms of the variable $\boldsymbol{\mu} \in \Lambda$. Inserting (3.11) into (3.10), one obtains an optimization problem for the variable $\boldsymbol{\mu} \in \Lambda$ that reads:

$$\sup_{\boldsymbol{\mu} \in \Lambda} \left[-\frac{g^2}{2r} \int_{\Omega} |\boldsymbol{\mu}|^2 dx + \frac{g}{r} \int_{\Omega} \mathbf{X}^n \cdot \boldsymbol{\mu} dx \right],$$

or equivalently,

$$\inf_{\boldsymbol{\mu} \in \Lambda} \left[\frac{1}{2} \int_{\Omega} |\boldsymbol{\mu}|^2 dx - \frac{1}{g} \int_{\Omega} \mathbf{X}^n \cdot \boldsymbol{\mu} dx \right]. \quad (3.12)$$

Another *Uzawa iterative algorithm* is advocated for the solution of (3.12) in order to take into account the non-smooth constraint in the definition of the set Λ . Namely, we introduce the Lagrangian \mathcal{L} defined by:

$$\mathcal{L}(\boldsymbol{\mu}, m) = \frac{1}{2} \int_{\Omega} |\boldsymbol{\mu}|^2 dx - \frac{1}{g} \int_{\Omega} \mathbf{X}^n \cdot \boldsymbol{\mu} dx + m \left(\int_{\Omega} |\boldsymbol{\mu}| dx - 1 \right), \quad (3.13)$$

where $m \geq 0$ is a scalar *Kuhn-Tucker* multiplier. The solution of (3.12) therefore corresponds to finding a saddle-point of the Lagrangian (3.13), that is to find $\boldsymbol{\xi}^n \in (L^2(\Omega))^2$ and $l^n \in \mathbb{R}_+$, such that

$$\mathcal{L}(\boldsymbol{\xi}^n, m) \leq \mathcal{L}(\boldsymbol{\xi}^n, l^n) \leq \mathcal{L}(\boldsymbol{\mu}, l^n), \quad \forall \boldsymbol{\mu} \in (L^2(\Omega))^2, \forall m \in \mathbb{R}_+. \quad (3.14)$$

Again, we advocate an (embedded) Uzawa-type method. The corresponding algorithm reads as follows: let $l^{n,0} \in \mathbb{R}_+$ be given; for $k \geq 0$, $l^{n,k}$ being known:

(Step 1) Solve

$$\boldsymbol{\xi}^{n,k} = \arg \inf_{\boldsymbol{\mu} \in (L^2(\Omega))^2} \left[\frac{1}{2} \int_{\Omega} |\boldsymbol{\mu}|^2 dx - \frac{1}{g} \int_{\Omega} \mathbf{X}^n \cdot \boldsymbol{\mu} dx + l^{n,k} \int_{\Omega} |\boldsymbol{\mu}| dx \right]. \quad (3.15)$$

Problem (3.15) admits a closed form solution, defined point-wise by:

$$\boldsymbol{\xi}^{n,k}(\mathbf{x}) = \left(\frac{1}{g} - \frac{l^{n,k}}{|\mathbf{X}^n(\mathbf{x})|} \right)^+ \mathbf{X}^n(\mathbf{x}), \quad a.e. \text{ on } \Omega, \quad (3.16)$$

where $(p)^+ = \max(p, 0)$.

(Step 2) Update

$$l^{n,k+1} = \max \left\{ 0, l^{n,k} + \rho \left(\int_{\Omega} |\boldsymbol{\xi}^{n,k}| dx - 1 \right) \right\}, \quad (3.17)$$

where $\rho > 0$ is a given positive parameter (sufficiently small).

Remark 3.1. When $k \rightarrow \infty$, (3.16) leads to

$$\boldsymbol{\xi}^n(\mathbf{x}) = \left(\frac{1}{g} - \frac{l^n}{|\mathbf{X}^n(\mathbf{x})|} \right)^+ \mathbf{X}^n(\mathbf{x}), \quad a.e. \text{ on } \Omega,$$

and combining this relation with (3.11) leads to an explicit formulation of $\mathbf{p}^n(\mathbf{x})$, namely

$$\mathbf{p}^n(\mathbf{x}) = \frac{gl^n}{r \sup\{gl^n, |\mathbf{X}^n(\mathbf{x})|\}} \mathbf{X}^n(\mathbf{x}).$$

Thus we can note that, when $gl^n > |\mathbf{X}^n(\mathbf{x})|$, the parameter g disappears in the expression of the final solution.

3.4. On the solution of the sub-problem (3.6)

Problem (3.6) can be written as follows: find $\mathbf{u}^n \in \mathbf{V}_f$ satisfying

$$r \int_{\Omega} \mathbf{u}^n \cdot \mathbf{v} d\mathbf{x} + \int_{\Omega} \nabla \mathbf{u}^n : \nabla \mathbf{v} d\mathbf{x} = \int_{\Omega} (r\mathbf{p}^n - \boldsymbol{\lambda}^n) \cdot \mathbf{v} d\mathbf{x}, \quad \forall \mathbf{v} \in \mathbf{V}_0,$$

where $\mathbf{V}_0 = \{\mathbf{v} \in (H^1(\Omega))^2 : \nabla \cdot \mathbf{v} = 0\}$, and $\mathbf{S} : \mathbf{T} = \sum_{i,j=1}^2 s_{ij}t_{ij}$, for all $\mathbf{S} = (s_{ij}) \in \mathbb{R}^{2 \times 2}$, $\mathbf{T} = (t_{ij}) \in \mathbb{R}^{2 \times 2}$. From a computational point of view, we introduce a (*pressure-like*) multiplier $p^n \in L^2(\Omega)$ and consider the equivalent formulation: find $\{\mathbf{u}^n, p^n\} \in (H^1(\Omega))^2 \times L^2(\Omega)$ satisfying, for all $\mathbf{v} \in (H^1(\Omega))^2$ and $q \in L^2(\Omega)$

$$r \int_{\Omega} \mathbf{u}^n \cdot \mathbf{v} d\mathbf{x} + \int_{\Omega} \nabla \mathbf{u}^n : \nabla \mathbf{v} d\mathbf{x} - \int_{\Omega} p^n \nabla \cdot \mathbf{v} d\mathbf{x} = \int_{\Omega} (r\mathbf{p}^n - \boldsymbol{\lambda}^n) \cdot \mathbf{v} d\mathbf{x}, \tag{3.18a}$$

$$\int_{\Omega} \nabla \cdot \mathbf{u}^n q d\mathbf{x} = \int_{\Omega} f q d\mathbf{x}. \tag{3.18b}$$

Remark 3.2. Problem (3.18) is the weak formulation of a *generalized Stokes problem*, which has a unique solution in $(H^1(\Omega))^2 \times L^2(\Omega)$ [29, 31]. The strong formulation of this problem actually reads

$$\begin{cases} r\mathbf{u}^n - \nabla^2 \mathbf{u}^n + \nabla p^n = r\mathbf{p}^n - \boldsymbol{\lambda}^n & \text{in } \Omega, \\ \nabla \cdot \mathbf{u}^n = f & \text{in } \Omega, \\ \nabla \mathbf{u}^n \mathbf{n} - p^n \mathbf{n} = 0 & \text{on } \Gamma, \end{cases}$$

where \mathbf{n} is the outward unit normal vector at Γ .

The solution methods discussed for the Stokes problem with $f = 0$ still apply here. For instance, a *preconditioned conjugate gradient algorithm*, see, e.g., [31, Chapter 4], can be applied. A monolithic approach with stabilized piecewise linear finite element techniques [15, 16] is favored in the sequel for implementation convenience, and detailed in Section 4. Note that, as highlighted in [12] for similar problems from the calculus of variations, the choice of the solution method for the Stokes problem does not influence the behavior of the iteration algorithm (as seen for instance when replacing stabilized finite elements with the *mini-element* [32]). The use of low order finite element is appropriate for such non-smooth problems, for which the data and therefore the solution have low regularity properties.

4. Finite Element Approximation

4.1. Generalities

Finite element techniques are used for the computer implementation of algorithm (3.5)-(3.7). Let $h > 0$ be a discretization step. A family $\{\Omega_h\}_h$ of polygonal approximations of the domain Ω is introduced such that $\lim_{h \rightarrow 0} \Omega_h = \Omega$, together with $\lim_{h \rightarrow 0} \Gamma_h = \Gamma$. Next we consider a family $\{\mathcal{T}_h\}_h$ of triangulations of Ω_h , verifying the following (classical) assumptions (see, e.g., [33]): (i) all the triangles K of \mathcal{T}_h are closed, and $\bigcup_{K \in \mathcal{T}_h} K = \overline{\Omega}_h$; (ii) if K_1 and K_2 belong to \mathcal{T}_h then either $K_1 \cap K_2 = \emptyset$, or K_1 and K_2 have only a vertex in common or only a full edge in common; (iii) h is the length of the largest edge(s) of \mathcal{T}_h ; (iv) if θ_h is the smallest angle of \mathcal{T}_h , then $\inf_h \theta_h > 0$; and (v) all the vertices of \mathcal{T}_h located on Γ_h belong to Γ .

Let us denote by N_n the number of vertices of \mathcal{T}_h in $\overline{\Omega}_h$, and by K a generic element (triangle) of \mathcal{T}_h . Let \mathbb{P}_k be the space of polynomials of degree less than or equal to k . We will

approximate $H^1(\Omega)$, $L^\infty(\Omega)$ and $L^2(\Omega)$ by the finite element space defined by

$$V_h^1 = \left\{ \varphi \in C^0(\overline{\Omega_h}) : \varphi|_K \in \mathbb{P}_1, \forall K \in \mathcal{T}_h \right\}.$$

Let φ_j , $j = 1, \dots, N_n$ denote the piecewise affine finite element basis functions of V_h^1 , associated with the triangulation \mathcal{T}_h . The discrete sup-norm is defined as

$$\|\mathbf{q}\|_{\infty,h} = \max_{j=1,\dots,N_n} |\mathbf{q}(P_j)| = \max_{j=1,\dots,N_n} \sqrt{q_1^2(P_j) + q_2^2(P_j)},$$

where $\mathbf{q} = (q_1, q_2)^T$, and P_j is a vertex of \mathcal{T}_h , while the discrete L^2 -scalar product is given by

$$(\mathbf{p}_h, \mathbf{q}_h)_{0,h} = \frac{1}{3} \sum_{j=1}^{N_n} A_j \mathbf{p}_h(P_j) \cdot \mathbf{q}_h(P_j),$$

where A_j is the area of the polygon which is the union of those triangles of \mathcal{T}_h which have P_j as a common vertex. The corresponding norm is defined by $\|\mathbf{p}_h\|_{0,h} = \sqrt{(\mathbf{p}_h, \mathbf{p}_h)_{0,h}}$.

4.2. Discrete augmented lagrangian and saddle-point problem

The discrete equivalent to the augmented Lagrangian functional \mathcal{L}_r is given by

$$\begin{aligned} & \mathcal{L}_{r,h}(\mathbf{v}_h, \mathbf{q}_h; \boldsymbol{\mu}_h) \\ &= \frac{1}{2} \int_{\Omega_h} |\nabla \mathbf{v}_h|^2 d\mathbf{x} + g \|\mathbf{q}_h\|_{\infty,h} + \frac{r}{2} \|\mathbf{v}_h - \mathbf{q}_h\|_{0,h}^2 + (\boldsymbol{\mu}_h, \mathbf{v}_h - \mathbf{q}_h)_{0,h}. \end{aligned} \quad (4.1)$$

The discrete functional space corresponding to \mathbf{V}_f is given by

$$\mathbf{V}_{f,h} = \left\{ \mathbf{v}_h \in (V_h^1)^2 : \nabla \cdot \mathbf{v}_h \text{ is approximately equal to } f_h \text{ in } \Omega_h \right\},$$

where f_h is a suitable approximation of f (typically the interpolant of f that is piecewise constant on \mathcal{T}_h). We will detail a specific method to impose the divergence constraint at the discrete level when discussing later the method of approximation of the Stokes problems. The discrete saddle-point problem consists in looking for $\{\mathbf{u}_h, \mathbf{p}_h; \boldsymbol{\lambda}_h\} \in \mathbf{V}_{f,h} \times (V_h^1)^2 \times (V_h^1)^2$ such that

$$\mathcal{L}_{r,h}(\mathbf{u}_h, \mathbf{p}_h; \boldsymbol{\mu}_h) \leq \mathcal{L}_{r,h}(\mathbf{u}_h, \mathbf{p}_h; \boldsymbol{\lambda}_h) \leq \mathcal{L}_{r,h}(\mathbf{v}_h, \mathbf{q}_h; \boldsymbol{\lambda}_h), \quad (4.2)$$

for all $\{\mathbf{v}_h, \mathbf{q}_h; \boldsymbol{\mu}_h\} \in \mathbf{V}_{f,h} \times (V_h^1)^2 \times (V_h^1)^2$.

4.3. Discrete Uzawa algorithm

A discrete Uzawa-Douglas-Rachford type algorithm corresponding to (3.5)-(3.7) reads as follows: let $\mathbf{u}_h^{-1} \in \mathbf{V}_{f,h}$ and $\boldsymbol{\lambda}_h^0 \in (V_h^1)^2$ be arbitrary given functions. Then, for $n \geq 0$, $\{\mathbf{u}_h^{n-1}, \boldsymbol{\lambda}_h^n\}$ being known, the iterates \mathbf{p}_h^n , \mathbf{u}_h^n and $\boldsymbol{\lambda}_h^{n+1}$ are computed as follows:

(a) Solve

$$\mathbf{p}_h^n = \arg \min_{\mathbf{q}_h \in (V_h^1)^2} \mathcal{L}_{r,h}(\mathbf{u}_h^{n-1}, \mathbf{q}_h; \boldsymbol{\lambda}_h^n). \quad (4.3)$$

(b) Solve

$$\mathbf{u}_h^n = \arg \min_{\mathbf{v}_h \in \mathbf{V}_{f,h}} \mathcal{L}_{r,h}(\mathbf{v}_h, \mathbf{p}_h^n; \boldsymbol{\lambda}_h^n). \quad (4.4)$$

(c) Update the multipliers $\boldsymbol{\lambda}_h^n \in (V_h^1)^2$:

$$\boldsymbol{\lambda}_h^{n+1} = \boldsymbol{\lambda}_h^n + r(\mathbf{u}_h^n - \mathbf{p}_h^n), \quad (4.5)$$

until convergence is reached. Similarly, the stopping criterion is typically $\|\mathbf{u}_h^n - \mathbf{u}_h^{n-1}\|_{0,h} < \varepsilon$, where ε is a given tolerance.

4.4. On the solution of the sub-problem (4.3)

Let us define $\mathbf{X}_h^n := r\mathbf{u}_h^{n-1} + \boldsymbol{\lambda}_h^n \in (V_h^1)^2$. Problem (4.3) reads

$$\min_{\mathbf{q}_h \in (V_h^1)^2} \left[\frac{r}{2}(\mathbf{q}_h, \mathbf{q}_h)_{0,h} + g \|\mathbf{q}_h\|_{\infty,h} - (\mathbf{X}_h^n, \mathbf{q}_h)_{0,h} \right]. \tag{4.6}$$

Since $\|\mathbf{q}_h\|_{\infty,h} = \max_{\boldsymbol{\mu}_h \in \Lambda_h} (\boldsymbol{\mu}_h, \mathbf{q}_h)_{0,h}$, where

$$\Lambda_h = \{ \boldsymbol{\mu}_h \in (V_h^1)^2 : (|\boldsymbol{\mu}_h|, 1)_{0,h} \leq 1 \},$$

Eq. (4.6) is equivalent to

$$\min_{\mathbf{q}_h \in (V_h^1)^2} \left\{ \max_{\boldsymbol{\mu}_h \in \Lambda_h} \left[\frac{r}{2}(\mathbf{q}_h, \mathbf{q}_h)_{0,h} + g(\boldsymbol{\mu}_h, \mathbf{q}_h)_{0,h} - (\mathbf{X}_h^n, \mathbf{q}_h)_{0,h} \right] \right\},$$

Similarly to the continuous case, minimum and maximum operators commute; for a given $\boldsymbol{\mu}_h$, the solution of the minimization problem reads $\mathbf{p}_h(\boldsymbol{\mu}_h) = (\mathbf{X}_h^n - g\boldsymbol{\mu}_h)/r$. Inserting this explicit solution into the previous problem, one obtains an optimization problem for the variable $\boldsymbol{\mu}_h \in (V_h^1)^2$ that reads:

$$\min_{\boldsymbol{\mu}_h \in \Lambda_h} \left[\frac{1}{2}(\boldsymbol{\mu}_h, \boldsymbol{\mu}_h)_{0,h} - \frac{1}{g}(\mathbf{X}_h^n, \boldsymbol{\mu}_h)_{0,h} \right]. \tag{4.7}$$

The constraint $(|\boldsymbol{\mu}_h|, 1)_{0,h} \leq 1$ is taken into account with a *Kuhn-Tucker* multiplier $m_h \in \mathbb{R}_+$. The discrete *Uzawa algorithm* for the solution of (4.7) relies on the discrete Lagrangian \mathcal{L}_h defined by:

$$\mathcal{L}_h(\boldsymbol{\mu}_h, m_h) = \frac{1}{2}(\boldsymbol{\mu}_h, \boldsymbol{\mu}_h)_{0,h} - \frac{1}{g}(\mathbf{X}_h^n, \boldsymbol{\mu}_h)_{0,h} + m_h ((|\boldsymbol{\mu}_h|, 1)_{0,h} - 1). \tag{4.8}$$

The solution of (4.7) therefore corresponds to finding the saddle-point of the Lagrangian (4.8). The Uzawa algorithm reads as follows: let $l_h^{n,0} \in \mathbb{R}_+$ be given, and, for $k \geq 0$, $l_h^{n,k}$ being known:

(Step 1) Solve

$$\min_{\boldsymbol{\mu}_h \in (V_h^1)^2} \left[\frac{1}{2}(\boldsymbol{\mu}_h, \boldsymbol{\mu}_h)_{0,h} - \frac{1}{g}(\mathbf{X}_h^n, \boldsymbol{\mu}_h)_{0,h} + l_h^{n,k} (|\boldsymbol{\mu}_h|, 1)_{0,h} \right]. \tag{4.9}$$

Problem (4.9) admits a closed form solution, which is given by:

$$\boldsymbol{\xi}_h^{n,k} = \left(\frac{1}{g} - \frac{l_h^{n,k}}{|\mathbf{X}_h^n|} \right)^+ \mathbf{X}_h^n. \tag{4.10}$$

(Step 2) Update

$$l_h^{n,k+1} = \max \left\{ 0, l_h^{n,k} + \rho \left((|\boldsymbol{\xi}_h^{n,k}|, 1)_{0,h} - 1 \right) \right\}, \tag{4.11}$$

where $\rho > 0$ is a given positive parameter (sufficiently small).

4.5. On the solution of the sub-problem (4.4)

Problem (4.4) is equivalent to finding $\mathbf{u}_h^n \in \mathbf{V}_{f,h}$ satisfying

$$r(\mathbf{u}_h^n, \mathbf{v}_h)_{0,h} + \int_{\Omega} \nabla \mathbf{u}_h^n : \nabla \mathbf{v}_h \, d\mathbf{x} = (\mathbf{Y}_h^n, \mathbf{v}_h)_{0,h}, \quad \forall \mathbf{v}_h \in \mathbf{V}_{0,h},$$

where $\mathbf{V}_{0,h} = \{ \mathbf{v}_h \in (V_h^1)^2 : \nabla \cdot \mathbf{v}_h \text{ is approx. equal to } 0 \}$, and $\mathbf{Y}_h^n := r\mathbf{p}_h^n - \boldsymbol{\lambda}_h^n \in (V_h^1)^2$. We introduce a multiplier $p_h^n \in V_h^1$ to take into account the divergence constraint in the definition of $\mathbf{V}_{f,h}$. We add stabilization terms to make this choice of finite element spaces for $\{ \mathbf{u}_h^n, p_h^n \}$

a stable one. The finite element formulation considered here reads as follows: find $\{\mathbf{u}_h^n, p_h^n\} \in (V_h^1)^2 \times V_h^1$ satisfying

$$\begin{aligned} & r(\mathbf{u}_h^n, \mathbf{v}_h)_{0,h} + \int_{\Omega} \nabla \mathbf{u}_h^n : \nabla \mathbf{v}_h d\mathbf{x} - \int_{\Omega_h} p_h^n \nabla \cdot \mathbf{v}_h d\mathbf{x} + \int_{\Omega_h} \nabla \cdot \mathbf{u}_h^n q_h d\mathbf{x} + S_h(\mathbf{u}_h^n, p_h^n; \mathbf{v}_h, q_h) \\ & = (\mathbf{Y}_h^n, \mathbf{v}_h)_{0,h} + \int_{\Omega_h} f_h q_h d\mathbf{x} + T_h(\mathbf{Y}_h^n, f_h; \mathbf{v}_h, q_h), \end{aligned} \tag{4.12}$$

for all $\{\mathbf{v}_h, \mathbf{q}_h\} \in (V_h^1)^2 \times V_h^1$, and where (following [15])

$$S_h(\mathbf{u}_h^n, p_h^n; \mathbf{v}_h, q_h) := \sum_{K \in \mathcal{T}_h} \alpha h_K^2 \int_K \nabla p_h^n \cdot \nabla q_h d\mathbf{x}, \quad T_h(\mathbf{Y}_h^n, f_h; \mathbf{v}_h, q_h) \equiv 0,$$

where $\alpha \in \mathbb{R}_+$ ($\alpha = 1$ in the numerical experiments) is a given parameter and h_K is the *diameter* of the element K .

Remark 4.1. Following [16], another choice would be a *Galerkin Least-Squares*-type of stabilization method that reads:

$$\begin{aligned} S_h(\mathbf{u}_h^n, p_h^n; \mathbf{v}_h, q_h) & := \sum_{K \in \mathcal{T}_h} \alpha h_K^2 \int_K \nabla p_h^n \cdot \nabla q_h d\mathbf{x}, \quad T_h(\mathbf{Y}_h^n, f_h; \mathbf{v}_h, q_h) \\ & := \sum_{K \in \mathcal{T}_h} \alpha h_K^2 \int_K \mathbf{Y}_h^n \cdot \mathbf{v}_h d\mathbf{x}. \end{aligned}$$

Numerical experiments have shown similar results with both choices of stabilization terms.

Remark 4.2. Note that the numerical method for the solution of the Stokes problem can be replaced by any other solution method. In particular, the use of conjugate gradient algorithms, together with \mathbb{P}_1 -iso- $\mathbb{P}_2/\mathbb{P}_1$ finite element approximations, or the *mini element* (\mathbb{P}_1 -bubble/ \mathbb{P}_1) are other options described in [31] and [32]. Numerical results in [12] have shown convergence properties that are independent of the solution method for the Stokes problem, when applied to a related non-smooth eigenvalue problem.

Remark 4.3. When the function f presents some singularity, exact integration is needed to evaluate the right-hand side $\int_{\Omega_h} f_h q_h d\mathbf{x}$, as the classical trapezoidal formula cannot be used if the singularity coincides with a grid point. A method mixing numerical quadrature and exact integration is detailed in Appendix 7 for the case of f given by (2.11).

5. Numerical Results

We present numerical results for various choices of data f (smooth and non-smooth), and for the unit disk $\mathcal{D}_1 = \{\mathbf{x} = (x_1, x_2) \in \mathbb{R}^2 : x_1^2 + x_2^2 < 1\}$, and the unit square $\Omega_s = (0, 1) \times (0, 1)$. In the following numerical experiments, we have considered (unless specified otherwise) $r = 10$, $\varepsilon = 10^{-5}$ and $\rho = 1$.

5.1. Smooth data

Skipping the case $f = 0$ that naturally leads to the solution $\mathbf{u} = \mathbf{u}_h = \mathbf{0}$, we first consider a constant function f , namely $f = 2$. Fig. 5.1 visualizes the piecewise linear approximation \mathbf{u}_h of the solution \mathbf{u} to Eq. (2.3) obtained by the augmented Lagrangian approach for various mesh sizes when $f = 2$. Fig. 5.2 illustrates cuts of the Euclidean norm $|\mathbf{u}_h|_2 : \mathbf{x} \rightarrow \sqrt{u_{1h}^2(\mathbf{x}) + u_{2h}^2(\mathbf{x})}$

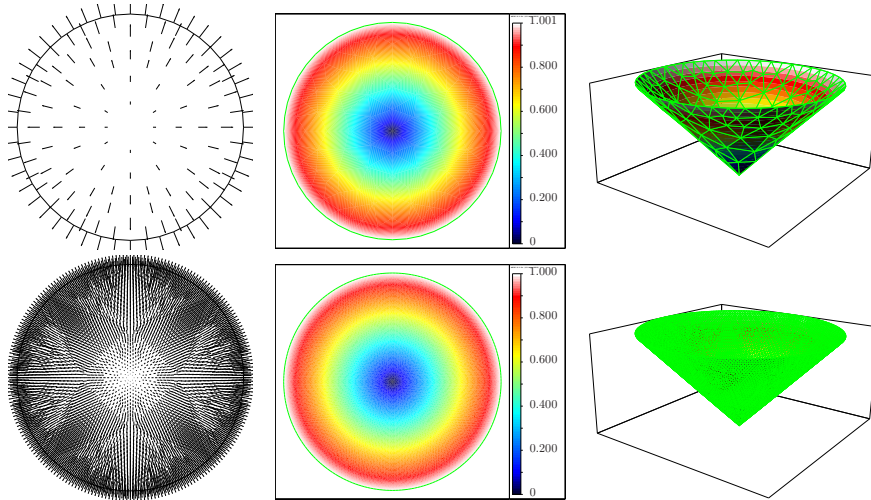


Fig. 5.1. Approximated solution \mathbf{u}_h (left), contours of $|\mathbf{u}_h|_2$ (middle), and graph of $|\mathbf{u}_h|_2$ (right) obtained with the augmented Lagrangian method on the unit disk \mathcal{D}_1 for $f = 2$ (first row: $h = 0.06942$, second row: 0.01285).

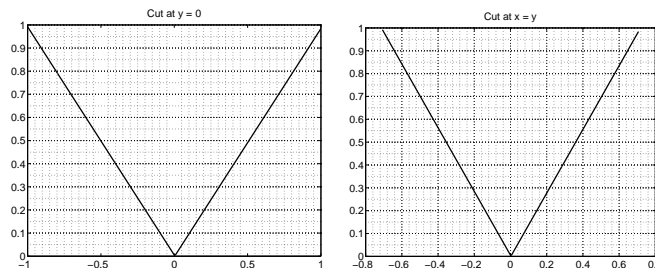


Fig. 5.2. Cuts of the graph of $|\mathbf{u}_h|_2$ along $x_2 = 0$ (left) and $x_1 = x_2$ (right) obtained with the augmented Lagrangian method on the unit disk \mathcal{D}_1 for $f = 2$ ($h = 0.06942$).

along the lines $x_2 = 0$ and $x_2 = x_1$, and confirms that the solution is a radial field centered around the origin (as stated in Proposition 2.1).

Following Proposition 2.1, and considering the field $\mathbf{u}_{\text{ex}}(x_1, x_2) = (x_1, x_2)^T$ as the exact solution on \mathcal{D}_1 , the convergence of the solution \mathbf{u}_h towards \mathbf{u}_{ex} is illustrated in Fig. 5.3 (left). It shows that $\|\mathbf{u}_h - \mathbf{u}_{\text{ex}}\|_{(L^2(\Omega))^2} = \mathcal{O}(h^2)$. Fig. 5.3 (middle) illustrates that $\nabla \cdot \mathbf{u}_h \rightarrow 2$ when $h \rightarrow 0$, and shows that

$$\|\nabla \cdot \mathbf{u}_h - f_h\|_\infty = \mathcal{O}(h^4).$$

Fig. 5.3 (right) illustrates the behavior of the sup-norm $\|\mathbf{u}_h\|_\infty$ as a function of h . One can observe that $\|\mathbf{u}_h\|_\infty \rightarrow 1$ when $h \rightarrow 0$ (as expected), with nearly second order accurate convergence. Table 5.1 contains the corresponding numerical values.

Remark 5.1. For $f = 2$, the solution obtained with the augmented Lagrangian approach is independent of the value of the parameter g appearing in the definition of $J(\cdot)$ in (2.3) (the parameter g varying in the range of $10^{-10} - 10^3$). Actually any (strictly positive) value of $g > 0$ is sufficient to force the solution to be bounded. In other words, the function $g \rightarrow \|\mathbf{u}_h\|_\infty$,

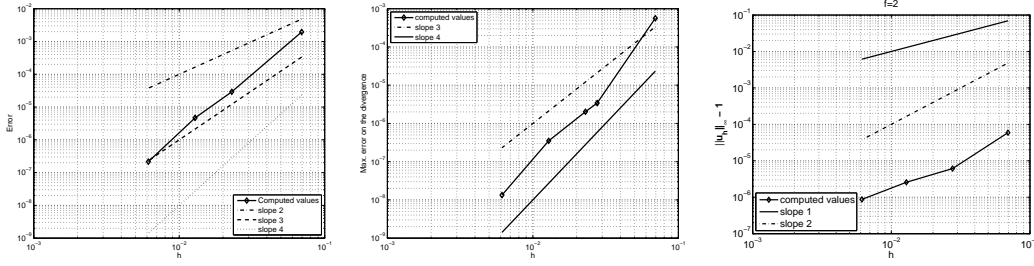


Fig. 5.3. Augmented Lagrangian algorithm: Case $f = 2$ and $\mathbf{u}_{\text{ex}}(x_1, x_2) = (x_1, x_2)^T$ on the unit disk. Left: Convergence (log-log plot) of the error $\|\mathbf{u}_h - \mathbf{u}_{\text{ex}}\|_{(L^2(\Omega))^2}$. Middle: Convergence (log-log plot) of the error $\|\nabla \cdot \mathbf{u}_h - f_h\|_\infty$. Right: Convergence (log-log plot) of the error $\|\mathbf{u}_h\|_\infty - 1$.

Table 5.1: Augmented Lagrangian algorithm: Case $f = 2$ and $\mathbf{u}_{\text{ex}}(x_1, x_2) = (x_1, x_2)^T$ on the unit disk. Convergence of the errors $\|\mathbf{u}_h - \mathbf{u}_{\text{ex}}\|_{(L^2(\Omega))^2}$, $\|\nabla \cdot \mathbf{u}_h - f_h\|_\infty$ and $\|\mathbf{u}_h\|_\infty - 1$.

h	$\ \mathbf{u}_h - \mathbf{u}_{\text{ex}}\ _{(L^2(\Omega))^2}$	$\ \nabla \cdot \mathbf{u}_h - f_h\ _\infty$	$\ \mathbf{u}_h\ _\infty - 1$
0.069422	$1.94750 \cdot 10^{-3}$	$5.63330 \cdot 10^{-4}$	$5.92519 \cdot 10^{-5}$
0.027670	$1.06827 \cdot 10^{-5}$	$3.40814 \cdot 10^{-6}$	$6.13026 \cdot 10^{-6}$
0.012846	$4.66425 \cdot 10^{-6}$	$3.51247 \cdot 10^{-7}$	$2.57716 \cdot 10^{-6}$
0.006137	$2.15005 \cdot 10^{-7}$	$1.33799 \cdot 10^{-8}$	$8.73001 \cdot 10^{-7}$

(where $\mathbf{u}_h = \mathbf{u}_h(g)$ is considered as a function of g) is constant. The same remark holds for the non-smooth functions f considered in the sequel.

Remark 5.2. When the function f is smooth (*i.e.* for instance $f \in C^0(\overline{\Omega})$), as it is the case for $f = 2$), the vector-valued field \mathbf{u} obtained by differentiating the solution $\Phi \in H^2(\Omega) \cap H_0^1(\Omega)$ of the potential problem $-\Delta \Phi = f$ coincides with the solution of the variational problem (2.3).

Remark 5.3. If $\mathbf{u} = (u_1, u_2)^T \in \mathbf{S}_f$ is the solution of (2.3), numerical experiments show that it satisfies:

$$\sup_{\mathbf{x} \in \Omega} \text{ess } u_i(\mathbf{x}) + \inf_{\mathbf{x} \in \Omega} \text{ess } u_i(\mathbf{x}) = 0, \quad i = 1, 2. \tag{5.1}$$

This property can be easily verified analytically when the norm on $C^0(\overline{\Omega})$ is given by $\|\mathbf{v}\|_\infty := \max_{\mathbf{x} \in \overline{\Omega}} \max\{|v_1(\mathbf{x})|, |v_2(\mathbf{x})|\}$. It is also satisfied numerically when using the norm $\|\mathbf{v}\|_\infty = \max_{\mathbf{x} \in \overline{\Omega}} \sqrt{|v_1(\mathbf{x})|^2 + |v_2(\mathbf{x})|^2}$. To show that relation (5.1) holds with the norm $\|\cdot\|_\infty$ replacing the norm $\|\cdot\|_\infty$ that is used in the computations, let us define $\alpha_i = \sup_{\mathbf{x} \in \Omega} \text{ess } u_i(\mathbf{x}) + \inf_{\mathbf{x} \in \Omega} \text{ess } u_i(\mathbf{x})$, for $i = 1, 2$. Assume that $\alpha_i \neq 0$, $i = 1, 2$. In that case, define $\bar{\mathbf{u}} = (\bar{u}_1, \bar{u}_2)^T$ such that $\bar{u}_i = u_i - \alpha_i$, $i = 1, 2$, and verify that $\|\nabla \bar{\mathbf{u}}\|_{L^2(\Omega)} = \|\nabla \mathbf{u}\|_{L^2(\Omega)}$, and in turn that $\|\bar{\mathbf{u}}\|_\infty < \|\mathbf{u}\|_\infty$. This implies that $J(\bar{\mathbf{u}}) < J(\mathbf{u})$ and leads to a contradiction since \mathbf{u} is the minimizer of $J(\cdot)$.

Fig. 5.4 visualizes the piecewise linear approximation \mathbf{u}_h of the solution to Eq. (2.3) on the unit square Ω_s obtained by the augmented Lagrangian approach for various mesh sizes when $f = 2$. The solution is a radial field centered around $(0.5, 0.5)$ that agrees with Proposition 2.1. Fig. 5.5 shows the cuts of $|\mathbf{u}_h|_2$ along the lines $x_2 = 1/2$ and $x_1 = x_2$, and confirms the radial invariance of the solution.

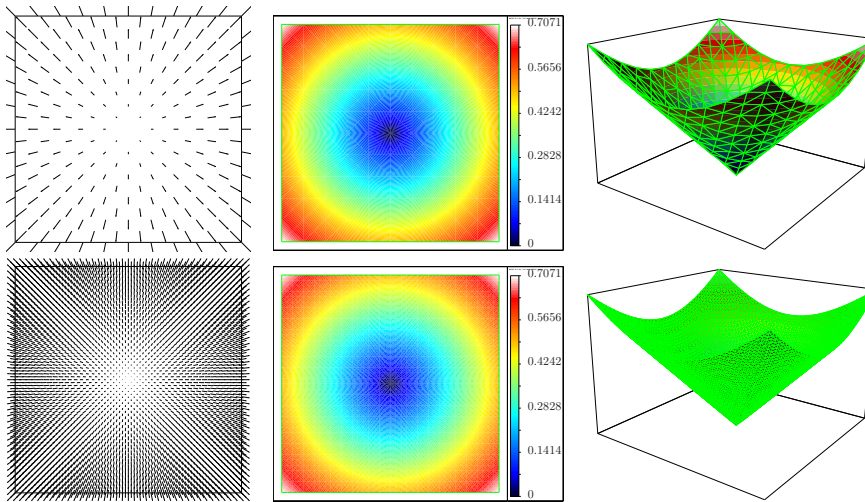


Fig. 5.4. Field \mathbf{u}_h (left), contours of $|\mathbf{u}_h|_2$ (middle), and graph of $|\mathbf{u}_h|_2$ (right) obtained with the augmented Lagrangian method on the unit square Ω_s for $f = 2$ (first row: $h = 0.05$, second row: 0.0125).

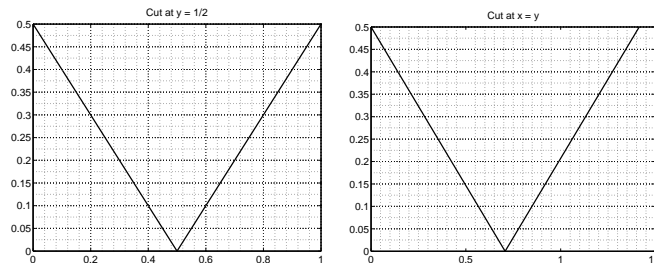


Fig. 5.5. Cuts of $|\mathbf{u}_h|_2$ along $x_2 = 1/2$ (left) and $x_1 = x_2$ (right) obtained with the augmented Lagrangian method on the unit square Ω_s for $f = 2$ ($h = 0.05$).

Fig. 5.6 finally shows the evolution of $J(\mathbf{u}_h^n)$ for the unit disk (left) and the unit square (right), J being the objective function and \mathbf{u}_h^n the n^{th} iterate produced by the discrete augmented Lagrangian algorithm (4.3)-(4.5); we took $\mathbf{u}_h^{-1} = \mathbf{0}$ and $\boldsymbol{\lambda}_h^0 = \mathbf{0}$ for both cases. Results confirm the convergence of $J(\mathbf{u}_h^n)$ in less than 20 iterations for both cases.

5.2. Non-smooth data with point singularity: the case $f \in L^2(\Omega)$

Let us consider now the case (2.11) with $s \leq 1$. If $s < 1$, we have $f \in L^2(\Omega)$, and Theorem 2.1 holds. Actually, when $s = 1$, $f \notin L^2(\Omega)$ and, a priori, the general theory from [1, 2] does not apply. However, we will see in Section 5.4 that the numerical method we advocate is still constructive if $s = 1$.

The *quasi-exact integration* detailed in Appendix 7 is used, with $N_i = 3$, to compute the integrals in the right-hand side, for elements K adjacent to the singularity point when the singularity point coincides with a grid point. Fig. 5.7 shows the solution obtained for the unit disk \mathcal{D}_1 , $(x_1^0, x_2^0) = (0, 0)$, and $s = 3/4$. Instabilities develop near the singularity point. It also visualizes cuts of the graph of $|\mathbf{u}_h|_2$ along the line $x_2 = x_1$, and shows that the oscillations

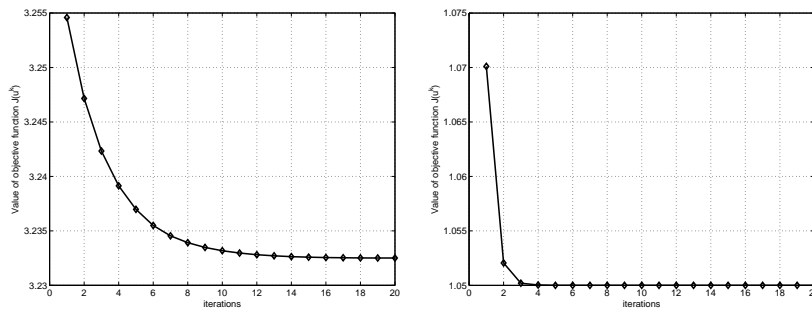


Fig. 5.6. Evolution of objective function $J(\mathbf{u}_h^n)$ for $f = 2$ on the unit disk ($h = 0.06942$) (left) and the unit square Ω_s ($h = 0.05$) (right). The initial data are $\mathbf{u}_h^{-1} = \mathbf{0}$ and $\lambda_h^0 = \mathbf{0}$.

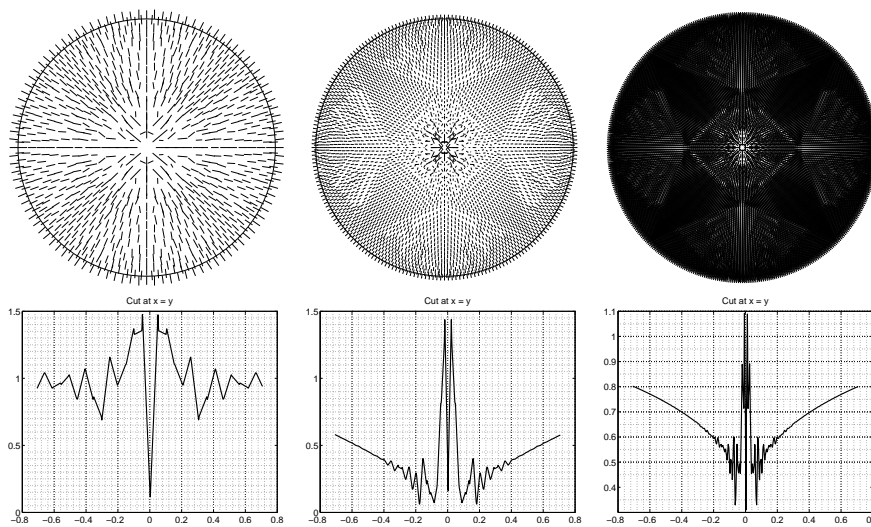


Fig. 5.7. Approximation \mathbf{u}_h obtained with the augmented Lagrangian method on the unit disk \mathcal{D}_1 for the function $f(x_1, x_2) = (\sqrt{x_1^2 + x_2^2})^{-3/4}$ ($s = 3/4$), for $h = 0.069422, 0.022983, \text{ and } 0.012846$ (left to right). Top row: field \mathbf{u}_h ; bottom row: cut of the graph of $|\mathbf{u}_h|_2$ along $x_1 = x_2$.

concentrate at the singularity point when $h \rightarrow 0$. Observe that we have been able to 'capture' the solution when it does not belong to $C^0(\overline{\Omega})$ but to $L^\infty(\Omega)$, only.

Remark 5.4. Our numerical experiments show that the quality of the solution is pretty much independent of the number of integration points if $N_i > 2$. Thus, we used $N_i = 3$ integration points for our computations.

In Fig. 5.8, we have shown the behavior of the sup-norm $\|\mathbf{u}_h\|_\infty$ for $f = r^{-s}$, $0.25 \leq s \leq 1$, as a function of the exponent s (with quasi-exact integration of the singularity and $N_i = 3$). We observe that $\|\mathbf{u}\|_\infty$ remains bounded even when $s = 1$, i.e. when f loses the L^2 -regularity.

In Fig. 5.9, we have visualized the approximate solution associated with the unit disk \mathcal{D}_1 for $s = 0.95, 0.75, 0.5, 0.25, 0.1$, respectively. One can observe that wiggles arise for all values of $s > 0$, even though they are smaller when $s \rightarrow 0$. Indeed, when $s \rightarrow 0$, $f \rightarrow 1$, and the data and the problem become smooth. The solution associated to $f = 1$ being $\mathbf{u}_1(x_1, x_2) =$

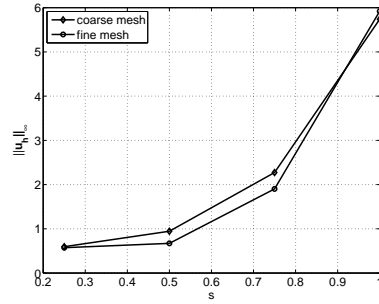


Fig. 5.8. Norm $\|\mathbf{u}_h\|_\infty$ of the solution obtained with the augmented Lagrangian method on the unit disk \mathcal{D}_1 with $f = r^{-s}$, as a function of the exponent s ($h \simeq 0.0276$ and $h \simeq 0.0128$).

$(x_1/2, x_2/2)^T$, one can observe in Fig. 5.8 that $\|\mathbf{u}_h\|_\infty \rightarrow 1/2$ when $s \rightarrow 0$ as expected, since $\|\mathbf{u}_1\|_\infty = 1/2$.

We can investigate the convergence properties of the solution in the case $f(\mathbf{x}) = 1/|\mathbf{x}|^s$ on the unit disk, in a similar fashion as the analysis in the smooth case presented in Fig. 5.3. Let us consider $f(x_1, x_2) = r^{-s}$, with $r = \sqrt{x_1^2 + x_2^2}$; following Proposition 2.1, we compare the approximated solution \mathbf{u}_h with

$$\mathbf{u}_{\text{ex}}(x_1, x_2) = \frac{1}{r^s} \frac{1}{2-s} \begin{pmatrix} x_1 \\ x_2 \end{pmatrix} \tag{5.2}$$

on the unit disk \mathcal{D}_1 . When $s = 1$, the solution is in $L^\infty(\Omega)^2$ (but not in $C^0(\overline{\Omega})^2$), despite the fact that $f \notin L^2(\Omega)$. The numerical experiment results reported in Fig. 5.10 suggest the following convergence behavior: When $f(r) = r^{-s}$, with $s \in (0, 1]$, the approximated solution \mathbf{u}_h satisfies the following error estimate: there exists a constant C independent of the mesh size h such that

$$\|\mathbf{u}_h - \mathbf{u}_{\text{ex}}\|_{(L^2(\Omega))^2} \leq Ch^{2-s},$$

where \mathbf{u}_{ex} is the exact solution given by Proposition 2.1 and (5.2). This figure includes the case $s = 1$, even though f does not have the regularity required in [1,2] (the case $s = 1$ is treated in Section 5.4).

5.3. Non-smooth data with line singularity : regularization approach

Let us consider the (smooth) function f_ε defined by

$$f_\varepsilon(\mathbf{x}) = f_\varepsilon(x_1, x_2) = \frac{1}{((x_1 - x_1^0)^2 + \varepsilon)^{s/2}}, \tag{5.3}$$

where $\varepsilon > 0$ is a small parameter, $s > 0$, and x_1^0 such that there exists x_2^0 with $(x_1^0, x_2^0) \in \Omega$: the function f_ε defined by (5.3) is obtained by *regularization* of the non-smooth function $f : (x_1, x_2) \rightarrow ((x_1 - x_1^0)^2)^{-s/2}$, which exhibits a singularity along the line $x_1 = x_1^0$. We take typically $\varepsilon = h^2$, so that the regularization effect takes place on a layer whose thickness is of the order of h . Note that, when $s = 1$, the singular function f satisfies $f(x_1, x_2) = |x_1 - x_1^0|^{-1/2}$ that is $f \in L^q(\Omega)$, for all $q < 2$, while $f \in L^2(\Omega)$ if $s < 1$.

Fig. 5.11 illustrates the results for the unit square Ω_s , $x_1^0 = 0.5$, $s = 0.5$, $\varepsilon = h^2$, and for various values of h . We perform 100 iterations of the augmented Lagrangian algorithm. We

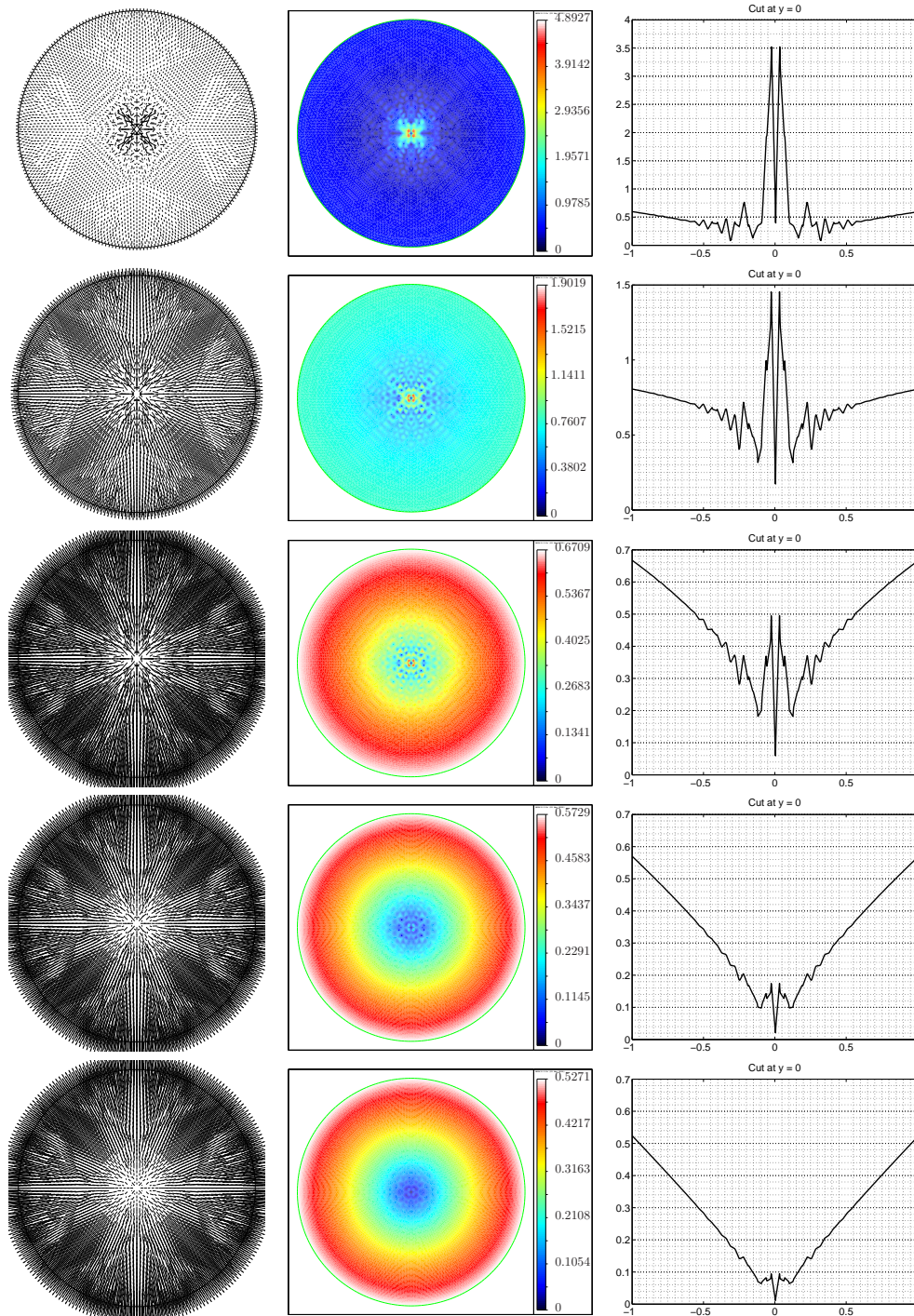


Fig. 5.9. Approximation \mathbf{u}_h obtained with the augmented Lagrangian method on the unit disk \mathcal{D}_1 for $f(r) = r^{-s}$ and $h = 0.0128$. Left: field \mathbf{u}_h ; middle: contours of the norm $|\mathbf{u}_h|_2$; right: cuts of $|\mathbf{u}_h|_2$ along $x_2 = 0$; From top to bottom: $s = 0.95, 0.75, 0.5, 0.25$ and 0.1 .

h	$\ \mathbf{u}_h - \mathbf{u}_{\text{ex}}\ _{(L^2(\Omega))^2}$	
	$s = 1$	$s = 0.75$
0.027670	1.27557163	0.49507782
0.012846	0.59638842	0.18807742
0.006137	0.28059914	0.07397987
	$s = 0.5$	$s = 0.25$
0.027670	0.20282001	0.08627280
0.012846	0.06267206	0.02172444
0.006137	0.02064375	0.00601491

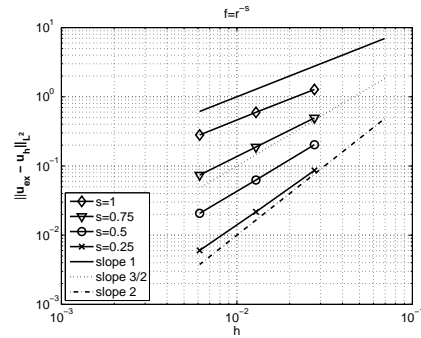


Fig. 5.10. Augmented Lagrangian algorithm: Case $f(r) = r^{-s}$ and $\mathbf{u}_{\text{ex}}(x_1, x_2) = \frac{1}{r^s} \frac{1}{2-s} (x_1, x_2)^T$ on the unit disk. Convergence of the error $\|\mathbf{u}_h - \mathbf{u}_{\text{ex}}\|_{(L^2(\Omega))^2}$ for $s = 1, 0.75, 0.5, 0.25$. Left: numerical values; right: plot on log-log scale.

observe that, when h is large, the regularization is important, leading to a function f_ε that is smooth, and a corresponding solution that is nearly radial. When h decreases, a discontinuity line takes place at $x_1 = x_1^0$. Boundary effects appear at the top and bottom of the domain. Cuts along the line $x_2 = 0.5$ illustrate the axial symmetry, but also the lack of radial symmetry of the solution; this becomes clearer when $h \rightarrow 0$. The smaller h , the slower the convergence of the augmented Lagrangian algorithm; indeed, typically, after 100 iterations, the residual $\|\mathbf{u}^{100} - \mathbf{u}^{99}\|_{(L^2(\Omega))^2}$ is smaller than 10^{-8} when $h \sim 10^{-1}$ and between 10^{-3} and 10^{-2} when $h \sim 10^{-4}$.

In conclusion, the regularization approach converges when $h \rightarrow 0$ and is numerically consistent. The convergence is slow since the data becomes singular; this behavior shows the

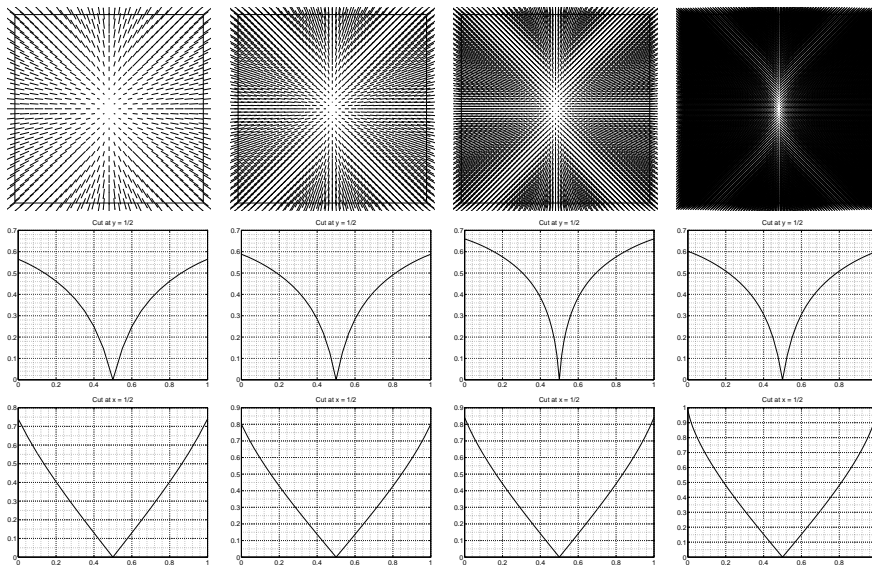


Fig. 5.11. Approximation \mathbf{u}_h obtained with the augmented Lagrangian method on the unit square Ω_s (top) and cuts of $|\mathbf{u}_h|_2$ along $x_2 = 1/2$ (middle) and $x_1 = 1/2$ (bottom), for f_ε given by (5.3) with $s = 1/2$, $\varepsilon = h^2$ and $x_1^0 = 0.5$. Left to right: $h = 5 \cdot 10^{-2}, 3.33 \cdot 10^{-2}, 2.50 \cdot 10^{-2}$ and $6.25 \cdot 10^{-3}$.

importance of designing exact or quasi-exact integration methods as those in Appendix 7.

5.4. Non-smooth data with point singularity: the case $f \notin L^2(\Omega)$

Let us turn back to the non-smooth case (2.11) with $s = 1$. As specified earlier, $f \notin L^2(\Omega)$ in this case. However, the numerical results presented below show that the augmented Lagrangian algorithm succeeds in finding a bounded solution to (2.1).

Fig. 5.12 shows the solution obtained for the unit disk \mathcal{D}_1 and $(x_1^0, x_2^0) = (0, 0)$. Instabilities develop near the singularity point. It also visualizes cuts of the graph of $|\mathbf{u}_h|_2$ along the line $x_2 = x_1$, and shows that the oscillations concentrate at the singularity point when $h \rightarrow 0$.

Fig. 5.8 actually shows that the sup-norm $\|\mathbf{u}_h\|_\infty$ increases exponentially when $s \rightarrow 1$, but remains bounded. Fig. 5.10 shows that, for this non-smooth problem, the order of the error $\|\mathbf{u}_h - \mathbf{u}_{\text{ex}}\|_{L^2(\Omega)^2}$ is consistent with the value of s in the definition of f ($f(r) = r^{-s}$). Convergence order for the approximation of the solution \mathbf{u}_h is obtained, also in this case with less regularity.

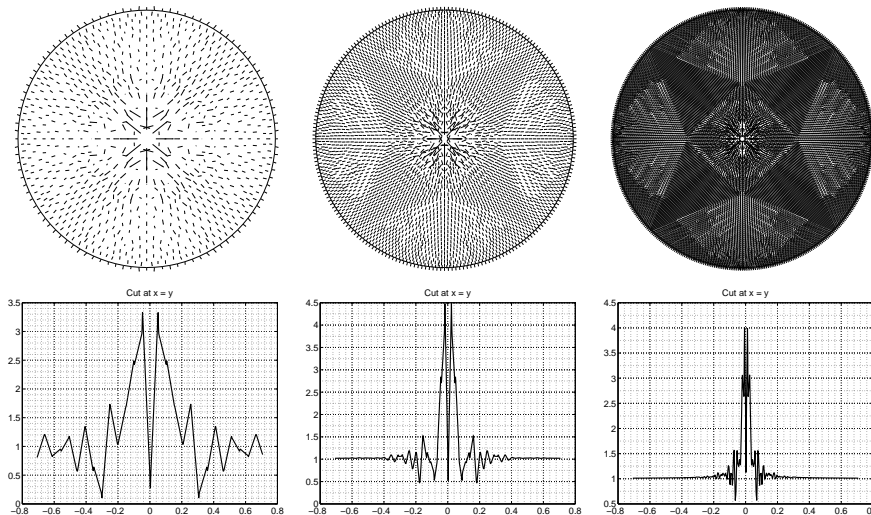


Fig. 5.12. Approximation \mathbf{u}_h obtained with the augmented Lagrangian method on the unit disk \mathcal{D}_1 for the function $f(x_1, x_2) = (x_1^2 + x_2^2)^{-1/2}$ ($s = 1$), for $h = 0.069422, 0.022983, \text{ and } 0.012846$ (left to right). Top row: fields \mathbf{u}_h ; bottom row: cuts of the graph of $|\mathbf{u}_h|_2$ along $x_1 = x_2$.

Numerical experiments for various functions f (smooth, non-smooth, and even with less regularity than the L^2 -regularity) have shown the ability of the L^∞ -regularization at finding solutions to (2.1). However, the advocated augmented Lagrangian method is fairly complicated conceptually (albeit relatively easy to implement). A natural question is therefore: What happens when using a simpler regularization technique based, e.g., on a L^2 -regularization? The answer to this question is the topic of Section 6.

6. L^2 -Regularization of the Divergence Equation

6.1. Model problem and generalities

Relaxing the condition $\mathbf{u} \in (C^0(\bar{\Omega}))^2$, we consider the following variant of problem (2.3):

$$\text{Find } \mathbf{u} \in \mathbf{T}_f \text{ such that } \frac{1}{2} \int_{\Omega} |\nabla \mathbf{u}|^2 d\mathbf{x} \leq \frac{1}{2} \int_{\Omega} |\nabla \mathbf{v}|^2 d\mathbf{x}, \quad \forall \mathbf{v} \in \mathbf{T}_f, \tag{6.1}$$

where $\mathbf{T}_f = \{\mathbf{v} \in (H^1(\Omega))^2 : \nabla \cdot \mathbf{v} = f \text{ in } \Omega\}$. A priori, the solution to (6.1) is not in $(L^\infty(\Omega))^2$. By introducing a *Lagrange multiplier* $p \in L^2(\Omega)$, the Euler-Lagrange system associated with (6.1) correspond to solving the *Stokes type system*:

$$\left\{ \begin{array}{ll} \text{Find } (\mathbf{u}, p) \in (H^1(\Omega))^2 \times L^2(\Omega) \text{ such that} & \\ -\nabla^2 \mathbf{u} + \nabla p = \mathbf{0} & \text{in } \Omega, \\ \nabla \cdot \mathbf{u} = f & \text{in } \Omega, \\ \frac{\partial \mathbf{u}}{\partial \mathbf{n}} - p \mathbf{n} = \mathbf{0} & \text{on } \partial\Omega, \end{array} \right. \tag{6.2}$$

where \mathbf{n} is the outward unit normal vector at $\partial\Omega$. Problem (6.2) is not well-posed as the unknown \mathbf{u} (the equivalent of a 'velocity') is defined up to an additive constant vector. Let γ be a positive constant. A simple way to force uniqueness is to replace (6.2) by:

$$\left\{ \begin{array}{ll} \text{Find } (\mathbf{u}_\gamma, p_\gamma) \in (H^1(\Omega))^2 \times L^2(\Omega) \text{ such that} & \\ -\nabla^2 \mathbf{u}_\gamma + \gamma \mathbf{u}_\gamma + \nabla p_\gamma = \mathbf{0} & \text{in } \Omega, \\ \nabla \cdot \mathbf{u}_\gamma = f & \text{in } \Omega, \\ \frac{\partial \mathbf{u}_\gamma}{\partial \mathbf{n}} - p_\gamma \mathbf{n} = \mathbf{0} & \text{on } \partial\Omega, \end{array} \right. \tag{6.3}$$

Problem (6.3) is well-posed; actually, it corresponds to replacing (6.1) by

$$\text{Find } \mathbf{u}_\gamma \in \mathbf{T}_f \text{ such that } J_\gamma(\mathbf{u}_\gamma) \leq J_\gamma(\mathbf{v}), \quad \forall \mathbf{v} \in \mathbf{T}_f, \tag{6.4}$$

where

$$J_\gamma(\mathbf{v}) = \frac{1}{2} \int_{\Omega} |\nabla \mathbf{v}|^2 d\mathbf{x} + \frac{\gamma}{2} \int_{\Omega} |\mathbf{v}|^2 d\mathbf{x}.$$

A priori, the solution to (6.4) is not in $(L^\infty(\Omega))^2$. We are interested in computing the solution of (6.4) for small values of the parameter $\gamma > 0$, and to study the convergence of \mathbf{u}_γ when $\gamma \rightarrow 0$.

6.2. Numerical algorithm and finite element discretization

Problem (6.3) is solved with stabilized piecewise linear finite element techniques, like those used to solve problem (4.4) in Section 4.5. Let $\mathbf{u}_{\gamma,h} \in (V_h^1)^2$ and $p_{\gamma,h} \in V_h^1$ be approximations of \mathbf{u}_γ and p_γ respectively. The finite element formulation considered here reads as follows:

Find $\{\mathbf{u}_{\gamma,h}, p_{\gamma,h}\} \in (V_h^1)^2 \times V_h^1$ such that

$$\begin{aligned} \gamma(\mathbf{u}_{\gamma,h}, \mathbf{v}_h)_{0,h} + \int_{\Omega} \nabla \mathbf{u}_{\gamma,h} : \nabla \mathbf{v}_h d\mathbf{x} - \int_{\Omega_h} p_{\gamma,h} \nabla \cdot \mathbf{v}_h d\mathbf{x} + \int_{\Omega_h} \nabla \cdot \mathbf{u}_{\gamma,h} q_h d\mathbf{x} \\ + \sum_{K \in \mathcal{T}_h} \alpha h_K^2 \int_K \nabla p_{\gamma,h} \cdot \nabla q_h d\mathbf{x}, = \int_{\Omega_h} f_h q_h d\mathbf{x}, \end{aligned} \tag{6.5}$$

for all $\{\mathbf{v}_h, q_h\} \in (V_h^1)^2 \times V_h^1$. Numerical results obtained by solving (6.5) are shown in Section 6.3.

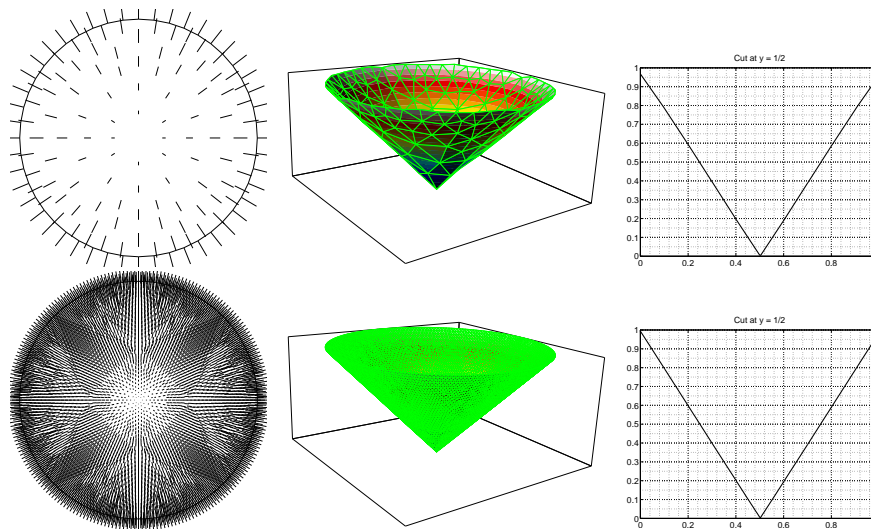


Fig. 6.1. Field \mathbf{u}_h (left), graph of $|\mathbf{u}_h|_2$ (middle), and cut of the graph of $|\mathbf{u}_h|_2$ according to $x_2 = 0$ (right) obtained with the L^2 -regularization approach ($\gamma = 10^{-3}$) on the unit disk \mathcal{D}_1 for $f = 2$ (first row: $h = 0.06942$, second row: 0.01285).

6.3. Numerical results

Smooth and non-smooth functions f are used to test the L^2 regularization approach, and the test cases from Section 5 are considered.

Smooth data. Fig. 6.1 illustrates the solution of (6.5) on the disk domain when $f = 2$. The computed results are *identical* to those obtained with the L^∞ -regularization (see Fig. 5.1). This is not surprising since both the data and the domain are very smooth.

Non-smooth data with point singularity (the case $f \in L^2(\Omega)$). Let us consider the (non smooth) case when f is given by (2.11) with $s = 0.75$. In Fig. 6.2, we have visualized the solution of (6.5) on the disk domain in that case, when using $\gamma = 10^{-3}$ as a regularization parameter; these results compare well with those in Fig. 5.7. The solution obtained with the L^2 -regularization method for different values of γ are very similar; moreover, they exhibit the same oscillations than the ones of the solution obtained with the L^∞ -regularization approach. Similar conclusions can be drawn with the data with a line singularity proposed in Section 5.3. In these cases, the L^2 -regularization allows to obtain bounded solutions even though not enforcing the L^∞ regularity explicitly.

Non-smooth data with point singularity (the case $f \notin L^2(\Omega)$). Let us finally consider the (even less smooth, and more interesting) case when f is given by (2.11) with $s = 1$. Fig. 6.3 illustrates the solution of (6.5) on the disk domain in that case, when using $\gamma = 10^{-3}$ as a regularization parameter; these results compare well with those in Fig. 5.12. However, in that case, the solution of the L^2 -regularized Eq. (6.3) depends on the value of the parameter γ ; indeed, numerical results reported in Fig. 6.4 shows that, for small values of γ ($\gamma \simeq 10^{-9}$) the solution changes drastically. On the other hand, for large values of γ , the solution is identical to the one obtained with the L^∞ -regularization. Results in Fig. 6.4 illustrates cuts of the graph of

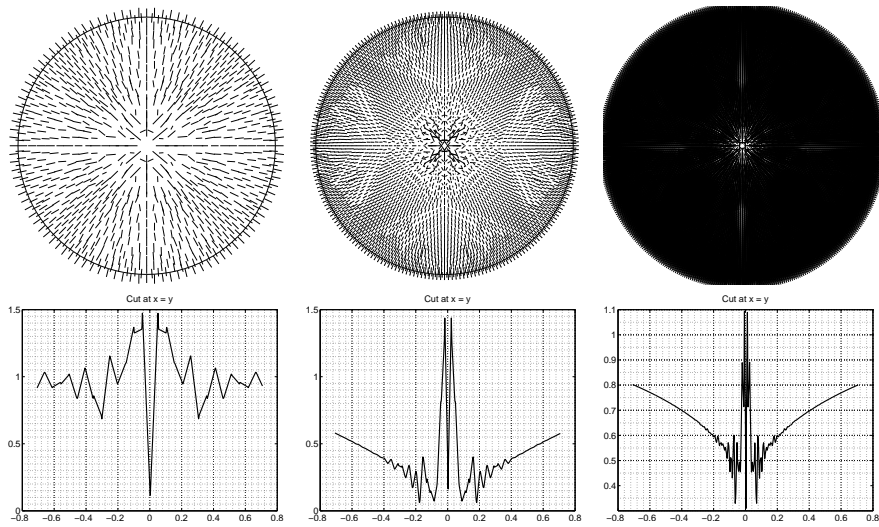


Fig. 6.2. Approximation \mathbf{u}_h obtained with the L^2 -regularization method ($\gamma = 10^{-3}$) on the unit disk \mathcal{D}_1 for the function $f(x_1, x_2) = (\sqrt{x_1^2 + x_2^2})^{-3/4}$ ($s = 3/4$), for $h = 0.069422, 0.022983, \text{ and } 0.012846$ (left to right). Top row: fields \mathbf{u}_h ; bottom row: cuts of the graph of $|\mathbf{u}_h|_2$ along $x_1 = x_2$.

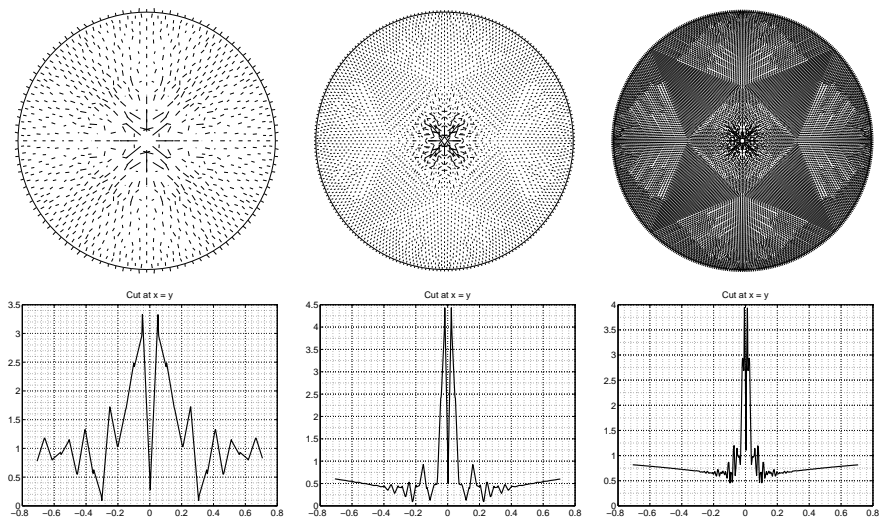


Fig. 6.3. Same as Fig. 6.2, except for the function $f(x_1, x_2) = (x_1^2 + x_2^2)^{-1/2}$ ($s = l$).

the norm $|\mathbf{u}_h|_2$ of the solution along $x_1 = x_2$ for various mesh sizes. The numerical results show the convergence when $h \rightarrow 0$, and show also that the maximum of the norm $|\mathbf{u}_h|_2$ is actually smaller when $\gamma = 10^{-9}$. Fig. 6.4 shows that, for a given value of γ , convergence is obtained when the mesh size tends to zero. On the other hand, there is no evidence to show that the limits \mathbf{u}_h when $h \rightarrow 0$ for different parameters γ are the same. This implies that an appropriate choice of the parameter γ is not guaranteed. Let us remark that this parameter dependence does not exist for the L^∞ -regularization method, as already emphasized in Remark 5.1. Therefore, the choice of the parameter γ is much more difficult to make than the choice for the parameter g

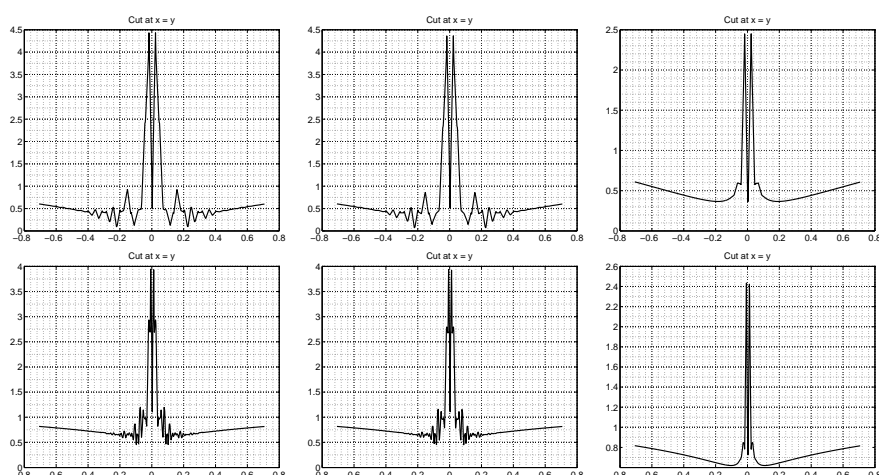


Fig. 6.4. Approximation \mathbf{u}_h obtained with the L^2 -regularization method. Cuts of the graph of $|\mathbf{u}_h|_2$ along $x_1 = x_2$ for $\gamma = 10^{-3}, 10^{-6}$ and 10^{-9} (top row: $h = 0.022983$, bottom row: $h = 0.012846$).

of the L^∞ -regularization method, and a systematic way of choosing γ is still an open question.

7. Conclusions

The approximation of the bounded solution of the divergence equation $\nabla \cdot \mathbf{u} = f$ has been investigated from the numerical viewpoint based on the introduction of regularizing L^∞ and L^2 terms in well-chosen functionals.

An augmented Lagrangian method for the L^∞ -based approach, together with piecewise linear finite elements, has been discussed. An Uzawa iterative algorithm allows to decouple nonlinearities and differential operators, requiring the solution of a sequence of local nonlinear problems and of generalized Stokes equations. A simpler regularization method based on a L^2 term has been considered and both approaches have been compared, leading to similar (but not always equal) solutions. Numerical results have been presented for various data, from smooth functions to functions with point or line singularities; they show good convergence properties. It is worth mentioning that the methods discussed in this article apply also to the numerical solution of (1.1) when f has less regularity than L^2 ; in this case, the approach based on a L^∞ -regularization is more robust.

Acknowledgments. The authors acknowledge the partial support of the National Science Foundation Grants NSF DMS-0412267 and NSF DMS-0913982. The authors thank Prof. H. Brezis (Rutgers University) for suggesting the investigation of this problem, Prof. Y. Maday (Université Paris VI) for pointing out reference [4], and M. Lewis (University of Houston) for implementation contributions. The first author gratefully acknowledges the partial support of Ycoor systems, Switzerland and of the Chair of numerical analysis and simulation, EPFL, Switzerland.

Appendix: Quasi-Exact Integration of Functions with Point Singularity

We consider $(x_1^0, x_2^0) \in \Omega$ and $f(x_1, x_2)$ given by (2.11). This function has a singularity at (x_1^0, x_2^0) . Let us consider a triangulation \mathcal{T}_h such that $P_0 := (x_1^0, x_2^0)$ is one grid point, and let us denote by φ_0 the piecewise linear finite element basis function associated to that node. In that case, one has to compute

$$d_0 := \int_{\Omega} f \varphi_0 d\mathbf{x} = \sum_{K \in \mathcal{T}_h, P_0 \in K} \int_K f \varphi_0 d\mathbf{x}.$$

On each triangle K which has P_0 as a vertex, one has $\varphi_0(x_1, x_2) = a(x_1 - x_1^0) + b(x_2 - x_2^0) + 1$, where $a, b \in \mathbb{R}$. Therefore

$$\begin{aligned} d_{0,K} &:= \int_K f \varphi_0 d\mathbf{x} \\ &= \int_K \frac{1}{((x_1 - x_1^0)^2 + (x_2 - x_2^0)^2)^{s/2}} (a(x_1 - x_1^0) + b(x_2 - x_2^0) + 1) dx_1 dx_2 \\ &= \int_K \frac{1}{r^s} (ar \cos \theta + br \sin \theta + 1) r dr d\theta \\ &= \int_{\theta_1}^{\theta_2} \int_0^{R(\theta)} \frac{1}{r^s} (ar \cos \theta + br \sin \theta + 1) r dr d\theta, \end{aligned} \tag{A.1}$$

with the polar change of variables $(x_1, x_2) = (x_1^0 + r \cos \theta, x_2^0 + r \sin \theta)$. Notation is illustrated in Fig. A.1.

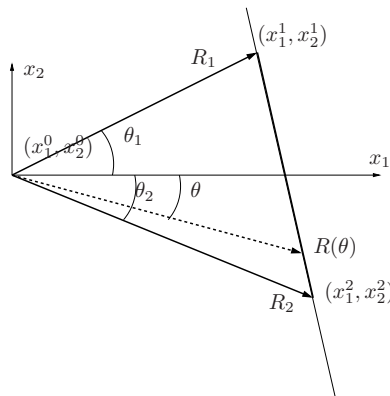


Fig. A.1. Exact integration on the triangle K . Sketch and notation.

Concerning the bounds of integration for the polar coordinates (r, θ) , the variable θ varies between the maximal and minimal angles θ_1 and θ_2 respectively. It remains to determine the upper bound $R(\theta)$ for the variable r . In order to do so, let us denote by $P_1 = (x_1^1, x_2^1)$ and $P_2 = (x_1^2, x_2^2)$ the other two vertices of K . The equation of the line going through P_1 and P_2 is $x_2 = x_2^1 + m(x_1 - x_1^1)$, where $m = (x_2^2 - x_2^1)/(x_1^2 - x_1^1)$. By using the change of variables, one obtains $r \sin \theta = x_2^1 - x_2^0 + m(r \cos \theta - (x_1^1 - x_1^0))$, and finally

$$r = R(\theta) = \frac{x_2^1 - x_2^0 - m(x_1^1 - x_1^0)}{\sin \theta - m \cos \theta}.$$

The integral (A.1) becomes, for $s < 1$,

$$\begin{aligned} d_{0,K} &= \int_{\theta_1}^{\theta_2} \int_0^{R(\theta)} (ar \cos \theta + br \sin \theta + 1) r^{1-s} dr d\theta \\ &= \int_{\theta_1}^{\theta_2} \int_0^{R(\theta)} (a \cos \theta r^{2-s} + b \sin \theta r^{2-s} + r^{1-s}) dr d\theta \\ &= \int_{\theta_1}^{\theta_2} \left(\frac{a \cos \theta}{3-s} R(\theta)^{3-s} + \frac{b \sin \theta}{3-s} R(\theta)^{3-s} + \frac{1}{2-s} R(\theta)^{2-s} \right) d\theta. \end{aligned}$$

Appropriate modifications are made when $s = 1$. Let us denote by $F(\theta)$ the function

$$F(\theta) = \frac{a \cos \theta}{3-s} R(\theta)^{3-s} + \frac{b \sin \theta}{3-s} R(\theta)^{3-s} + \frac{1}{2-s} R(\theta)^{2-s}.$$

In order to use a trapezoidal formula, let us introduce a partition of $[\theta_1, \theta_2]$ defined by $(\xi_j)_{j=1}^{N_i+1}$, with $\theta_1 = \xi_1 < \xi_2 < \dots < \xi_{N_i} < \xi_{N_i+1} = \theta_2$ (N_i is the number of discretization points). Therefore, the coefficient $d_{0,K}$ can be approximated by:

$$d_{0,K} = \int_{\theta_1}^{\theta_2} F(\theta) d\theta \simeq \sum_{j=1}^{N_i} \frac{\xi_{j+1} - \xi_j}{2} [F(\xi_j) + F(\xi_{j+1})],$$

by using a trapezoidal formula. It remains to determine the coefficients a and b . Note that the last coefficient is one since $\varphi_0(P_0) = 1$. In order to do so, we solve the 2×2 system:

$$a(x_1^1 - x_1^0) + b(x_2^1 - x_2^0) + 1 = 0, \quad a(x_1^2 - x_1^0) + b(x_2^2 - x_2^0) + 1 = 0,$$

whose solution is

$$b = \frac{x_1^1 - x_1^2}{(x_1^2 - x_1^0)(x_2^1 - x_2^0) - (x_1^1 - x_1^0)(x_2^2 - x_2^0)}, \quad a = \frac{-1 - b(x_2^1 - x_2^0)}{x_1^1 - x_1^0},$$

with the appropriate modifications if any of the denominators is vanishing.

References

- [1] J. Bourgain and H. Brezis, Sur l'équation $\operatorname{div} Y = f$, *C. R. Acad. Sci. Paris, Sér. I*, **334** (2002), 973–976.
- [2] J. Bourgain and H. Brezis, On the equation $\operatorname{div} Y = f$ and application to control of phases, *J. Amer. Math. Soc.*, **16**:2 (2003), 393–426.
- [3] L.C. Evans, *Partial Differential Equations*, American Mathematical Society, third edition, 2002.
- [4] Y. Maday, L^∞ -stable approximation of a solution to $\operatorname{div}(\mathbf{Y}) = f$ for $f \in L^2$ in two dimensions, *J. Sci. Comp.*, **28**:2/3 (2006), 451–458.
- [5] J. Bourgain, H. Brezis and P. Mironescu, Lifting in Sobolev spaces, *J. d'Analyse*, **80** (2000), 37–86.
- [6] D. Arnold, L. Scott and M. Vogelius, Regular inversion of the divergence operator with Dirichlet boundary condition on a polygon, *Ann. Sc. Norm. Pisa, Serie IV*, **15** (1988), 169–192.
- [7] T. Rivière and D. Ye, Resolutions of the prescribed volume form equation, *Nonlinear Differential Equations and Applications*, **3** (1996), 323–369.
- [8] D. Ornstein, A non-inequality for differential operators in the L^1 norm, *Arch. Rat. Mech. Anal.*, **11** (1962), 40–49.
- [9] E.J. Dean and R. Glowinski, An augmented Lagrangian approach to the numerical solution of the Dirichlet problem for the elliptic Monge-Ampère equation in two dimensions, *Electronic Transactions on Numerical Analysis*, **22** (2006), 71–96.
- [10] E.J. Dean and R. Glowinski, Numerical methods for fully nonlinear elliptic equations of the Monge-Ampère type, *Comp. Meth. Appl. Mech. Engrg.*, **195** (2006), 1344–1386.

- [11] A. Caboussat and R. Glowinski, Numerical solution of a variational problem arising in stress analysis : The vector case, *Discrete and Continuous Dynamical Systems - Series A*, **27**:4 (2010), 1447–1472.
- [12] A. Caboussat and R. Glowinski, Numerical methods for the vector-valued solutions of non-smooth eigenvalue problems, *J. Sci. Comp.*, **45**:1-3 (2010), 64–89.
- [13] A. Caboussat, R. Glowinski and V. Pons, An augmented Lagrangian approach to the numerical solution of a non-smooth eigenvalue problem, *J. Numer. Math.*, **17**:1 (2009), 3–26.
- [14] K. Majava, R. Glowinski and T. Kärkkäinen, Solving a non-smooth eigenvalue problem using operator-splitting methods, *International Journal of Computer Mathematics*, **84**:6 (2007), 825–846.
- [15] F. Brezzi and J. Pitkäranta, On the stabilization of finite element approximations of the Stokes equations, W. Hackbusch, editor, *Efficient Solutions of Elliptic Systems*, pages 11–19, Vieweg, 1984.
- [16] L.P. Franca and S.L. Frey, Stabilized finite element method: II. The incompressible Navier-Stokes equations, *Comp. Meth. Appl. Mech. Engrg*, **99** (1992), 209–233.
- [17] A. Caboussat, R. Glowinski and A. Leonard, Looking for the best constant in a Sobolev inequality: A numerical approach, *Calcolo*, **47**:4 (2010), 211–238.
- [18] A.K. Tikhonov and V.Y. Arsenin, *Solutions of Ill-Posed Problems*, Wiley, New York, 1977.
- [19] A.N. Tikhonov, The regularization of incorrectly posed problems, *Doklady Akad. Nauk. SSSR*, **153** (1963), 42–52.
- [20] R. Lattes and J.L. Lions, *Méthode de Quasi-Reversibilité et Applications*, Dunod, Paris, 1967.
- [21] H.W. Engl and C.W. Groetsch, editors, *Inverse and Ill-Posed Problems*, Academic Press, Orlando, 1987.
- [22] A. Neumaier, Solving ill-conditioned and singular linear systems: A tutorial on regularization, *SIAM Review*, **40**:3 (1998), 636–666.
- [23] D.P. O’Leary, Near-optimal parameters for Tikhonov and other regularization methods, *SIAM J. Sci. Comp.*, **23**:4 (2001), 1161–1171.
- [24] S. Kim, K. Koh, S. Boyd and D. Gorinevsky, ℓ_1 trend filtering, *SIAM Review*, **51**:2 (2009), 339–360.
- [25] M. Schmidt, G. Fung and R. Rosales, Fast optimization methods for l^1 regularization: A comparative study and two new approaches, *Proceedings of European Conference on Machine Learning*, pages 286–297, 2007.
- [26] A. Caboussat, R. Glowinski and V. Pons, Numerical methods for non-smooth l^1 optimization : Applications to free surface flows and image denoising, *Int. J. Numerical Analysis and Modeling*, **6**:3 (2009), 355–374.
- [27] R. Glowinski, J.L. Lions and R. Trémolières, *Numerical Analysis of Variational Inequalities*, North Holland, 1981.
- [28] R. Glowinski, *Numerical Methods for Nonlinear Variational Problems*, Springer-Verlag, New York, NY, 1984.
- [29] V. Girault and P.A. Raviart, *Finite Element Methods for Navier-Stokes Equations: Theory and Algorithms*, Springer Series in Computational Mathematics, Springer-Verlag, 1986.
- [30] R. Glowinski and P.L. Tallec, *Augmented Lagrangians and Operator-Splitting Methods in Non-linear Mechanics*, SIAM, Philadelphia, 1989.
- [31] R. Glowinski, Finite Element Methods For Incompressible Viscous Flow, volume IX of *Handbook of Numerical Analysis (P.G. Ciarlet, J.L. Lions eds)*, pages 3–1176, Elsevier, Amsterdam, 2003.
- [32] D.N. Arnold, F. Brezzi and M. Fortin, A stable finite element for the Stokes equations, *Calcolo*, **21**:4 (1984), 337–344.
- [33] P.G. Ciarlet, Basic error estimates for elliptic problems, P. Ciarlet and J. Lions, editors, *Handbook of Numerical Analysis*, volume II, pages 17–351, North-Holland, Amsterdam, 1991.